Technical Report ECOM-0138-19-T

HIGH-FREQUENCY TRANSISTOR MODELING FOR CIRCUIT DESIGN

C. E. L. Technical Report No. 205

Contract No. DAAB07-68-C-0138

DA Project No. 1 HO 62102 A042 01 02

Prepared by

A. B. Macnee
R. J. Talsky

COOLEY ELECTRONICS LABORATORY

Department of Electrical Engineering
The University of Michigan
Ann Arbor, Michigan

for

U. S. Army Electronics Command, Fort Monmouth, N. J.

ABSTRACT

It has been found that hybrid-pi or high-frequency T are inadequate high-frequency models for certain transistor types even though the models are supplemented by reasonable extrinsic elements. The hybrid-pi can be modified to model these transistors by replacing the $r_\pi C_\pi$ circuit by an RC ladder. Using a computer optimization program an optimal, N-lump model is generated. For the 2N918 transistor a two-lump model extends the frequency range of the hybrid-pi model to $f_T/2$. Typical circuit examples show most of the improvement in model performance can be obtained with a two-lump model.

FOREWORD

This work was supported in part by the United States Army Electronics Command, Fort Monmouth, N. J., under contract DA28-043-AMC01870(E). The report is based on a report submitted by R. J. Talsky in partial fulfillment of the requirements for the E. E. Degree, University of Michigan, 1969.

TABLE OF CONTENTS

LIST OF ILLUSTRATIONS

LIST OF ILLUSTRATIONS (Cont.)

LIST OF TABLES

1. Introduction

Analysis and synthesis of circuits containing bipolar transistors require suitable device models. For this purpose, the most popular high-frequency, incremental models are the hybrid-pi and the high-frequency T (Ref. 1, 2). Under the usual high-frequency assumptions these two models are equivalent as indicated in Fig. 1. The popularity of these models stems from their simplicity and the relatively good correspondence between elements of the models and the basic physical processes in the device. In particular, the capacities C_e and C_π each have two components: a barrier, or depletion layer, capacitance and a base charge, or diffusion, capacitance. In modeling the dynamics of the charge stored in the base by a single lumped capacitance, one neglects the distributed nature of the base charge. The excess phase factor $\exp(\frac{-ns}{\omega\alpha})$ multiplying the controlled source in each model is an attempt to include the first-order effects of the distributed nature of the base change. It also should be noted that these are models of the intrinsic devices; header capacities and lead inductances must be added to describe most packaged devices accurately.

For the circuit designer, determination of the model parameters for a particular transistor type can be a significant problem. Device manufacturers usually do not provide enough data to allow

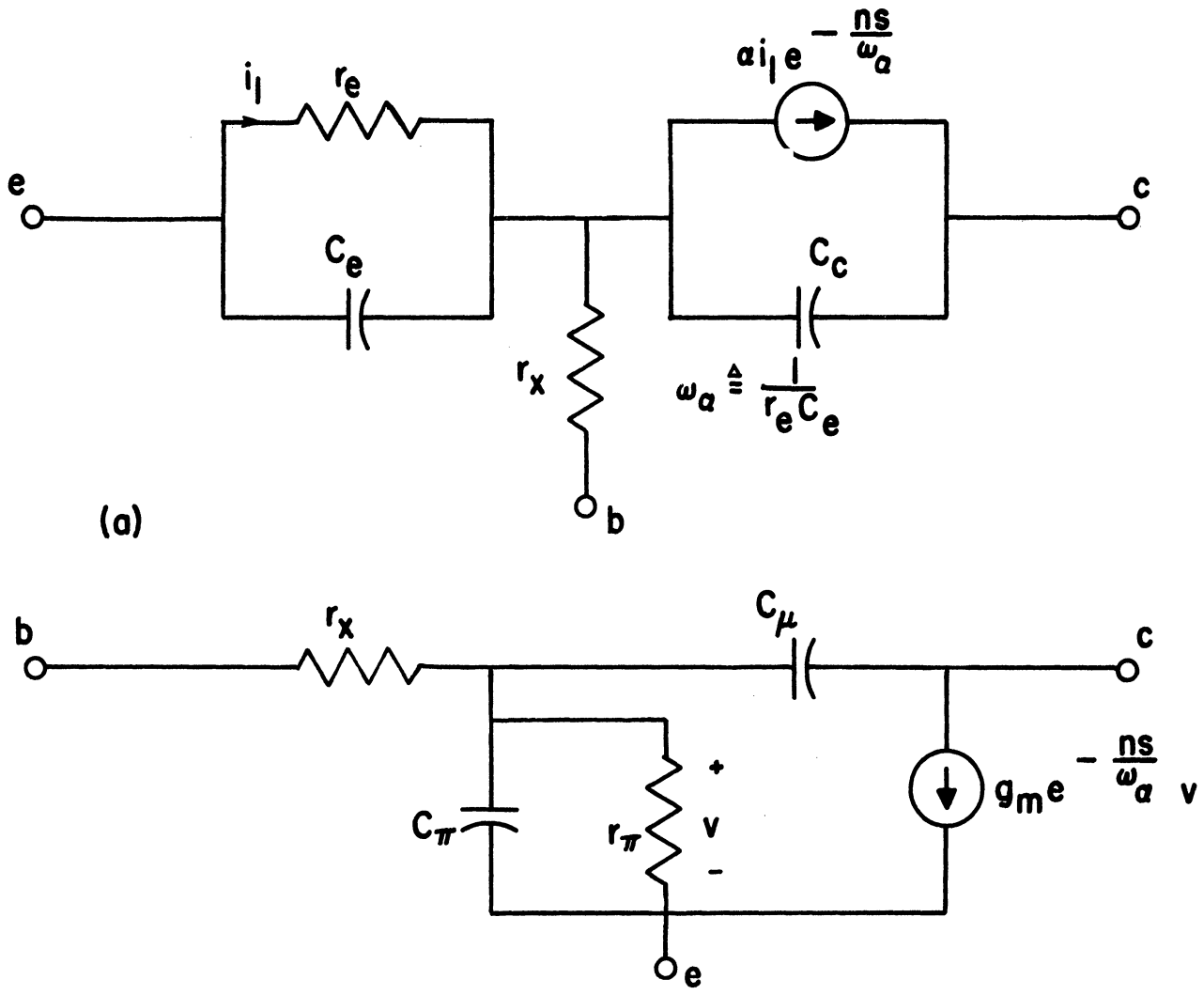

Fig. 1. Popular high-frequency, incremental models of a bipolar transistor; (a) high-frequency T and (b) high-frequency hybrid-pi and the parameter interrelations

calculation of all the parameters of the models in Fig. 1. The values for r_x, C_μ and n are particularly hard to find unless rather complete high-frequency data, such as a set of short-circuit admittance parameters, are provided. A perusal of manufacturer's data sheets reveals that extensive high-frequency data are available for a very limited number of devices. In 1966, Sidney Chao reported on the y-parameters of a collection of twenty transistor types produced by seven different manufacturers. That report seems to include most of the generally available data as of that date (Ref. 3).

In connection with wideband amplifier and oscillator studies, the writers had occasion to measure the short circuit admittance parameters of a small, planar, high-frequency transistor, the 2N918 (Appendix A). Analysis of this measured data revealed that using the circuits of Fig. 1, it was not possible to model this transistor satisfactorily over a frequency range greater than 0 to $0.1\, f_T$, even though extrinsic elements were added. The observed differences between the hybrid-pi model predictions and the measured data are most easily observed in plots of the short-circuit admittance loci, as indicated in the second section of this paper. These differences suggest that it is the "single-lump" representation of the distributed base charge which largely is responsible for the model's failure. In Section 3, two- and three-lump approximations to the distributed

base charge are added to the basic hybrid-pi, and a computer optimization program is used to select the parameters of this extended model. Finally, in Section 4 the responses of some typical circuits using the hybrid-pi and the extended hybrid-pi are compared. It is our conclusion that it is worthwhile to extend the hybrid-pi to a "two-lump" approximation, which requires the addition of one R and one C to the model. This extended model fits the 2N918 measured y-parameter data to within 10 percent up to about $f_T/2$, and can produce significant changes in the predicted response of typical circuits. The model can be extended further, but this does not seem to be worthwhile for the 2N918.

2. Admittance Loci

The short circuit admittance parameters of 2N918 transistors were measured over the frequency range 1 to 900 MHz for collector-emitter voltages from 1 to 8 V and collector currents from 0.5 to 8 mA. Some of the lowest frequency measurements were made with a Hewlett-Packard Vector voltmeter, but the bulk of the data was taken with a General Radio Transfer-Function and Immittance Bridge (50-900 Mhz range) and with a Boonton RX meter (10-200 MHz). In general there is good correspondence between the RX-meter and GR Bridge data over their common frequency range (50-200 MHz). These data are also qualitatively in good agreement with typical data published by manufacturers of this transistor type (Ref. 4). The inadequacy of the simple hybrid-pi model for this transistor is most easily seen if one examines the y_{ie} and y_{fe} admittance loci with frequency as a parameter. Figure 2 plots these loci using the data in the appendix for $V_{CE} = 4$ V and Ic = 0.5, 2.0 and 8.0 mA. It will be noted that the frequency at which $b_{ie}(\omega)$ reaches a maximum is much higher than the frequency at which $b_{fe}(\omega)$ is a minimum for each quiescent current. This is in conflict with the predictions of the usual hybrid-pi model.

The short circuit input and forward transfer admittances of the hybrid-pi model in Fig. 1(b) are

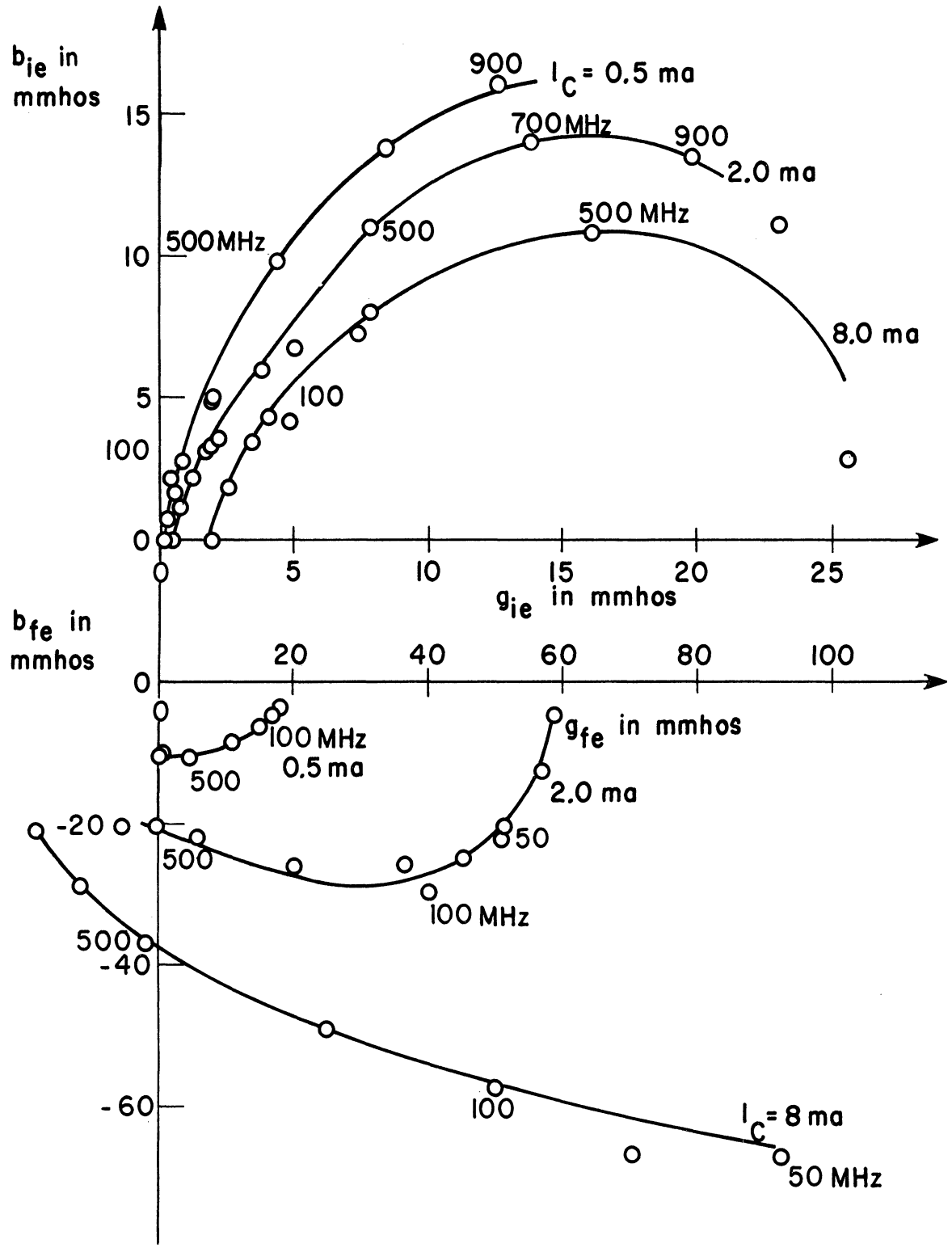

Fig. 2. Measured short circuit admittance loci for a 2N918 at V_{ce} = 4V

$$y_{ie} = \frac{1 + sr_\pi C_T}{r_x + r_\pi + sr_x r_\pi C_T} \tag{1}$$

and

$$y_{fe} = \frac{\beta e^{-\frac{ns}{\omega_\alpha}} - sr_\pi C_u}{r_x + r_\pi + sr_x r_\pi C_T} \tag{2}$$

where

$$C_T \triangleq C_\pi + C_u$$

Both of these admittances have the same pole at the transverse cut-off frequency

$$\omega_b \triangleq \frac{r_x + r_\pi}{r_x r_\pi C_T} \tag{3}$$

For $s = j\omega$, this pole dominates the frequency dependence of the susceptances

$$b_{ie}(\omega) = \frac{r_\pi^2 C_T}{(r_x + r_\pi)^2} \cdot \frac{\omega}{1 + \frac{\omega^2}{\omega_b^2}} \tag{4}$$

and

$$-b_{fe}(\omega) = \frac{g_m r_x r_\pi^2 C_T \omega \cos(\frac{n\omega}{\omega_\alpha}) + (r_x + r_\pi)[\omega r_\pi C_\mu + \beta \sin(\frac{n\omega}{\omega_\alpha})]}{(r_x + r_\pi)^2 (1 + \frac{\omega^2}{\omega_b^2})} \quad (5)$$

The value of ω_b is normally an order of magnitude smaller than ω_α, so that in the vicinity of ω_b the cosine and sine terms in (5) can be replaced by the first term in their respective power series. When this is done, Eq. 5 reduces to

$$-b_{fe}(\omega) = \frac{g_m r_x r_\pi^2 C_T + (r_x + r_\pi)(r_\pi C_\mu + \frac{n}{\omega\beta})}{(r_x + r_\pi)^2} \cdot \frac{\omega}{1 + \frac{\omega^2}{\omega_b^2}} \quad (6)$$

which has the same frequency dependence as $b_{ie}(\omega)$.

Equations (4) and (6) show that the hybrid-pi model predicts that the magnitude of b_{ie} and b_{fe} will both reach a maximum at the same frequency, ω_b. Further examination of Eqs. 1 and 2 shows that as long as the excess phase exponential is approximated by the first two terms in its series, both admittance loci are semicircles. Returning to the measured loci for the 2N918 it is evident that one can infer very different values for ω_b depending upon whether one uses the input or the transfer admittance locus. The frequencies of the various susceptance maximum are tabulated as follows:

	Frequency of Susceptance maxima		Frequency ratio
	b_{ie}	b_{fe}	
I_c = 0.5 mA	>900 MHz	500 MHz	>1.8
I_c = 2.0 mA	750 MHz	150 MHz	5
I_c = 8.0 mA	500 MHz	50	10

Since Fig. 1 and Eqs. 1 and 2 are for the intrinsic transistor, one is led naturally to ask if the observed differences between the model predictions and the measured data can be explained by extrinsic elements. It is our conclusion that this is not the case. The principal extrinsic elements are the bulk resistances, the lead inductances, and the interlead capacities.

Taken alone, the interlead capacities simply add linear susceptance terms to Eqs. 4 and 6. These can lead to susceptance maximum at differing frequencies, but nothing like the observed frequency ratios can be explained with reasonable capacity values. For example, subtracting the linear susceptance of 2 pF from the y_{ie} data at 8 mA only shifts the b_{ie} maximum frequency to about 450 MHz. Lead inductances can also cause some changes in the frequency of the susceptance maxima, but they tend to move the input susceptances down toward negative values at higher frequencies. There is

little evidence of this in the 2N918 data for the collector current and frequency ranges investigated.

The 2N918 is mounted in a standard TO-18 package. Measurements on such a package with the transistor disconnected give interlead capacities of the order of 0.6 pF between each pair of leads. Figure 3 replots the $y_{ie}(j\omega)$ locus for $I_c = 2.0$ mA, and shows the result of subtracting linear susceptances corresponding to 0.6, 1.2 and 1.8 pF.

It will be noted that even for the 1.8 pF case, which reduces the magnitude of the susceptance maximum by a factor of 2.2, the frequency of the maximum has only been reduced about 100 MHz to 650 MHz which is still 4.3 times the frequency of the transfer susceptance maximum.

The other interesting feature of these loci is their shape. Rather than being semicircles, as the hybrid-pi would predict, they look more like two semicircles joined by a tangent line. This observation naturally led to the consideration of the extension of the hybrid-pi to a two- or N-lump model.

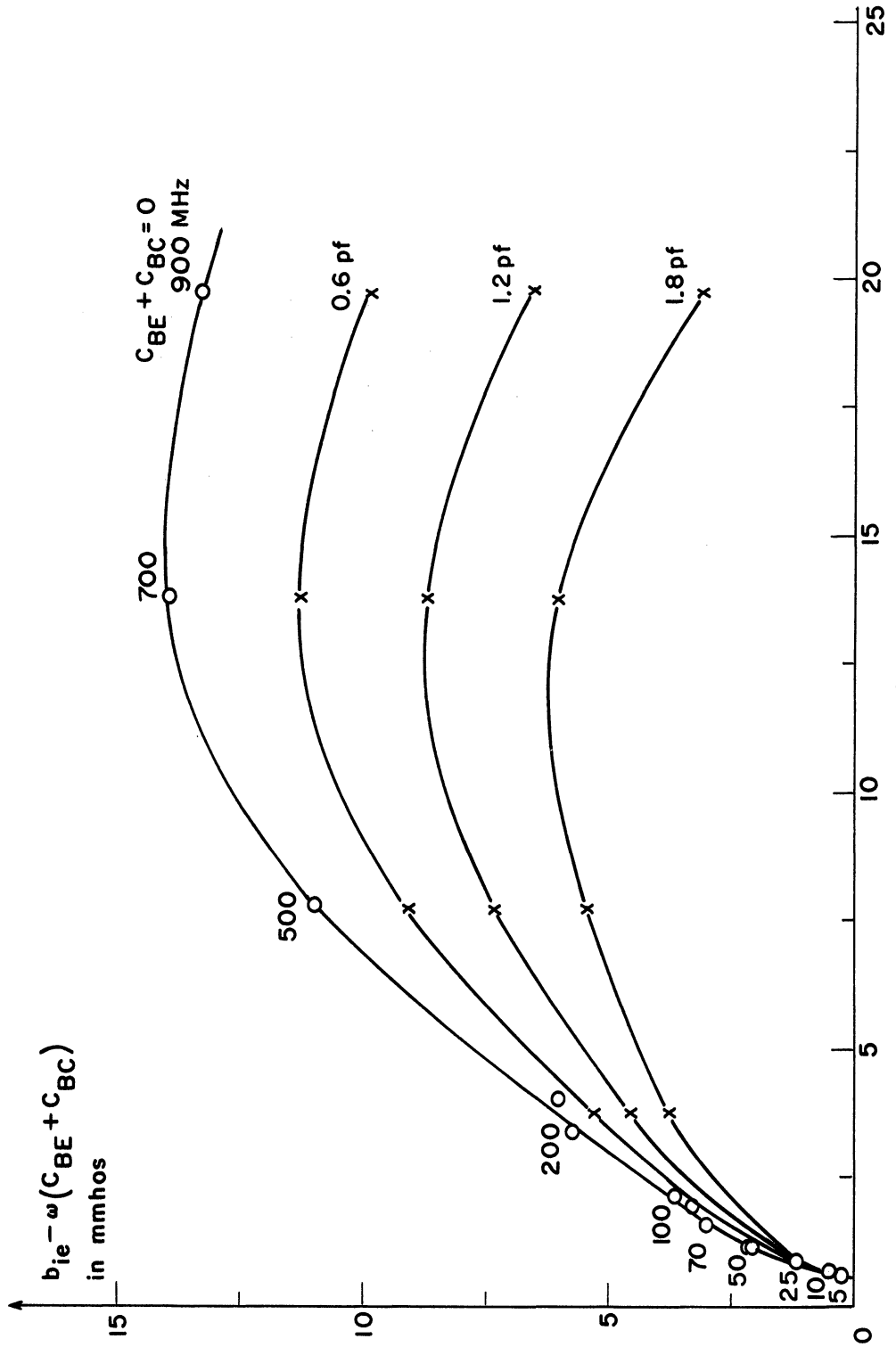

Fig. 3. Effect of interlead capacitances on the short circuit input admittance locus of 2N918 at $V_{ce} = 4V$ and $I_c = 2$ mA

3. Multilump Models

In the hybrid-pi model the dynamics of the minority charge diffusing across the base region of the transistor are modeled by the parallel $r_\pi C_\pi$ circuit. The element C_π also includes a component representing the barrier capacitance across the emitter-base space charge region, but for the usual emitter currents this term is dominated by the "diffusion" capacity. Physically, we know the diffusing charge is distributed across the base region, but both the hybrid-pi and the high-frequency T equivalent circuits treat this charge as though it were lumped at a single point. A distributed RC circuit could model the distributed charge exactly, but it would be awkward to use in circuit calculations. As an alternative it is natural to consider replacing the one-lump approximation to the distributed charge by a multilump approximation as shown in Fig. 4.

It is easily seen that introducing these RC ladder networks can give rise to differences between the driving-point and the transfer susceptance of the kind observed in the 2N918 measurements. The driving-point admittance has alternating simple zeros and poles along the negative real axis of the s-plane; whereas, if the voltage controlling the g_m-generator is taken from the end of the line, the transfer admittance is an all-pole function. By taking the g_m-generator control voltage at other points along the line one can introduce a

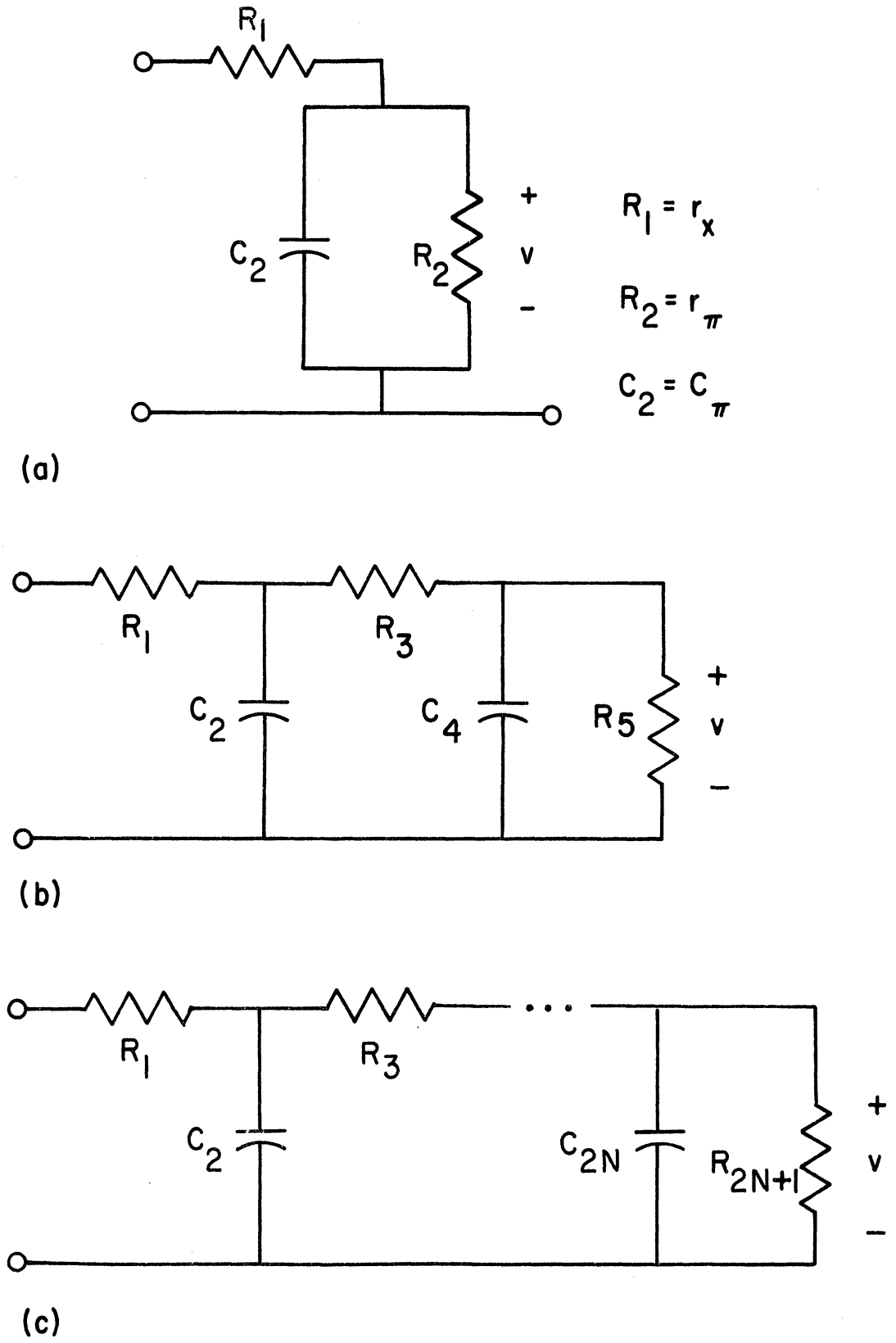

Fig. 4. One-, two- and N-lump models of distributed base charge

further degree of flexibility into the zeros of the transfer function.

Initially Bode plots of the y_{ie} and y_{fe} data were used to select the poles and zeros for a two-section ladder of the form shown in Fig. 4(b). With plots of the log magnitude and angle versus log frequency it is not difficult to make reasonable estimates of suitable asymptote break frequencies. Having the poles and zeros, it is a straightforward matter to synthesize the RC ladder. After several examples had been done "by hand," a digital computer program that selects the component values to minimize a suitable error measure was written.*

The error function selected is

$$\mathrm{ERR} = \sum_{\substack{\text{no. of} \\ \text{freq.}}} \left\{ W_1 \frac{\left| c_{y_{ie}}^{\text{data}} - c_{y_{ie}}^{\text{model}} \right|}{\left| c_{y_{ie}}^{\text{data}} \right|} \right\}^P + \left\{ W_2 \frac{\left| c_{y_{fe}}^{\text{data}} - c_{y_{fe}}^{\text{model}} \right|}{\left| c_{y_{fe}}^{\text{data}} \right|} \right\}^P \tag{7}$$

where W_1 and W_2 are weight constants, and P is a positive integer specified by the user. The quantities

---

*Appendix B gives the FORTRAN IV listing of this program.

$$^{c}y_{ie} \triangleq y_{ie} - s(C_{BE} + C_{BC}) \tag{8}$$

and

$$^{c}y_{fe} \triangleq y_{fe} + sC_{BC} \tag{9}$$

are the short-circuit input and forward transfer admittances of the intrinsic transistor, i.e., corrected for the interlead capacities C_{BE} and C_{BC}. The transfer and input admittances of the ladder network are evaluated efficiently by a simple cumulent algorithm (Ref. 5). The derivatives are estimated by incrementing element values in the simplest fashion.

A flow chart of the optimization program is given in Fig. 5. The program subtracts the admittances of the interlead capacities to obtain $^{c}y_{ie}$ and $^{c}y_{fe}$ of the intrinsic transistor. A Fletcher-Powell minimization routine is then used to minimize Eq. 7. The minimization routine is one given by Calahan (Ref. 6). A similar routine is available as a part of the IBM Scientific Subroutine Programs package (Ref. 7). When the minimization routine cannot reduce the error more than a specified percentage, the program adds the interlead capacities to the optimized model y-parameters and prints out the y-parameters and errors as a function of frequency as well as the "optimized" model values.

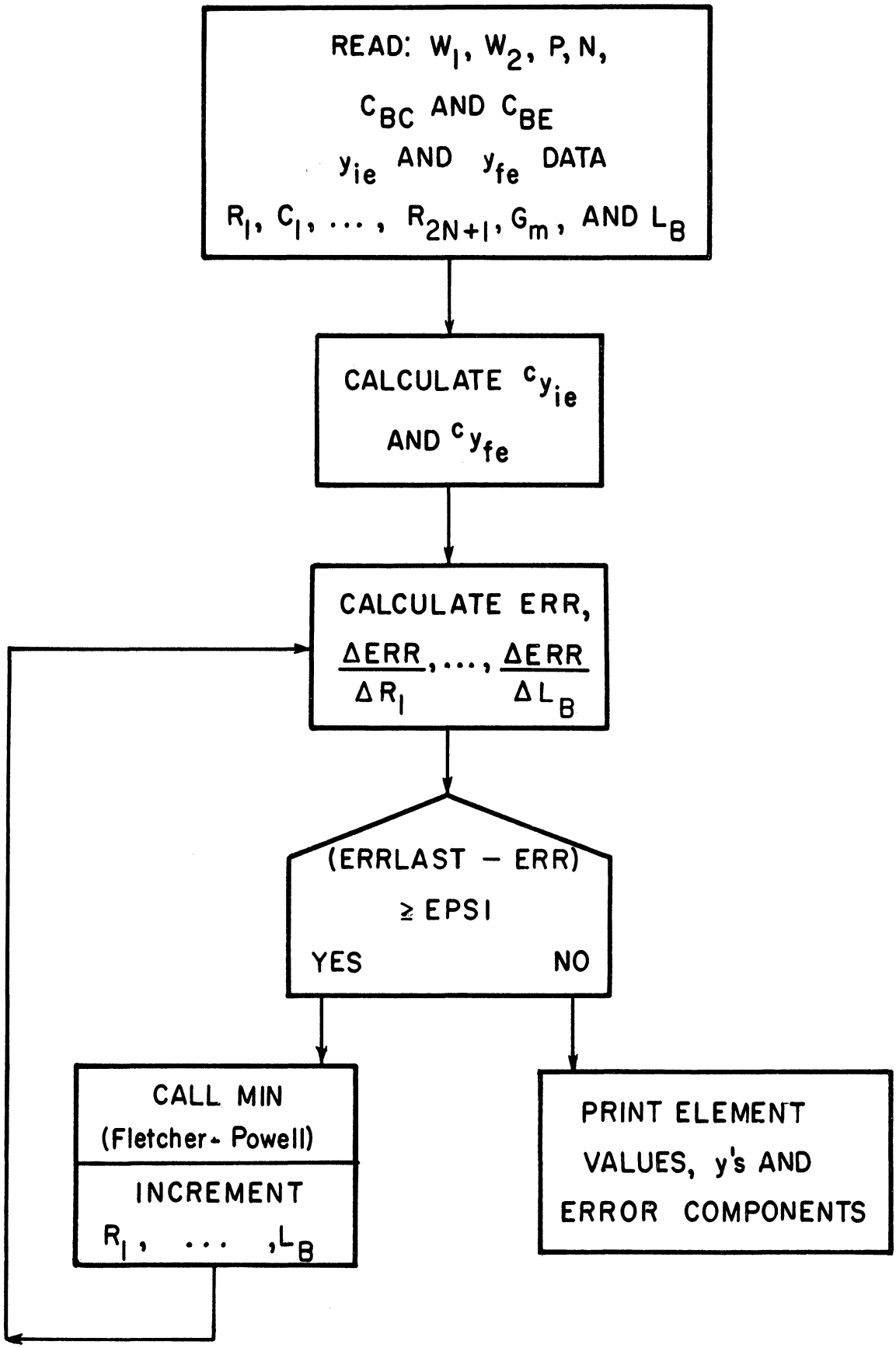

Fig. 5. Flow chart of transistor model optimization program

The complete N-lump transistor model is shown in Fig. 6(a). Our program optimizes R_1, C_2, ..., L_B to match the measured y_{ie} and y_{fe} data. The program could be extended to optimize simultaneously on all four y-parameters, but initial experience has suggested that this is often unnecessary because the output and reverse admittances are relatively independent of the stored-base charge.

When the collector-emitter terminals of the model are shorted, C_{CE} is removed from the circuit, C_μ is in parallel with C_2, and C_{BC} is in parallel with C_{BE} as shown in Fig. 6(b). The optimization program takes account of the specified C_{BC} and C_{BE}, but the C_2 it calculates includes C_μ. The y_{oe} and y_{re} data for the transistor are used to select C_{CE} and C_μ; at high frequencies

$$y_{re} \longrightarrow -sC_{BC} \tag{10}$$

and

$$y_{oe} \longrightarrow s\left(C_{CE} + C_{BC} + \frac{C_\mu C_2}{C_\mu + C_2}\right) \tag{11}$$

At low frequencies

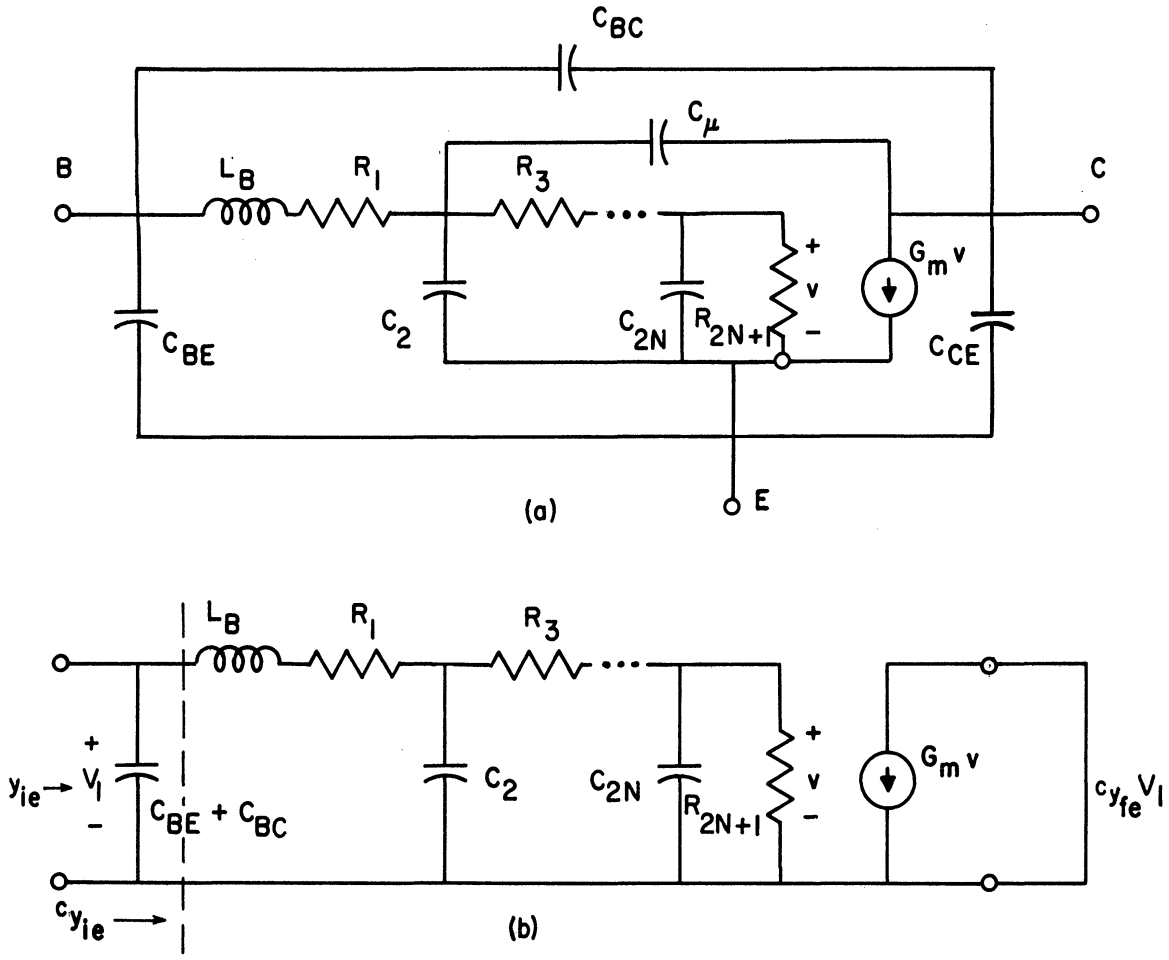

Fig. 6. (a) N-lump extension of hybrid-pi model plus extrinsic capacitances; (b) reduced model for y_{ie} and y_{fe} calculations

$$y_{re} \longrightarrow -s \left\{ C_{BC} + C_{\mu} \frac{R_3 + \ldots + R_{2N+1}}{R_1 + R_3 + \ldots + R_{2N+1}} \right\} \qquad (12)$$

and

$$y_{oe} \longrightarrow s \left\{ C_{CE} + C_{BC} + C_{\mu} \left[1 + \frac{g_m R_1 R_5}{R_1 + R_3 + \ldots + R_5} \right] \right\} \qquad (13)$$

In principle, having found the ladder element values R_1, C_2, ..., R_{2N+1} and G_m, Eqs. 10 and 11 can be used to determine C_{BC}, C_{CE}, and C_{μ}. As a practical matter, real data may not be precise enough at low frequencies to show a significant low frequency asymptote shift.

As an illustration, consider the 2N918 at $I_C = 2$ mA, $V_{CE} = 4$V. The y-parameter measured for one unit are tabulated in the appendix. The input and transfer-admittance loci for this transistor already have been presented in Fig. 2. The y_{oe} and y_{re} parameters, which are predominantly susceptive, are plotted in Fig. 7. Log-log coordinates are used so that the asymptotic susceptances are straight lines with a slope of +1. Looking at the data one cannot discern a significant difference between the low- and high-frequency susceptance asymptotes. The $-b_{re}$ data can be fitted very well by a single line corresponding to a capacity of 0.68 pF, and the b_{oe} data are well matched by a 1.63 pF capacity. On the basis of these data we can conclude for this transistor that C_{μ} is

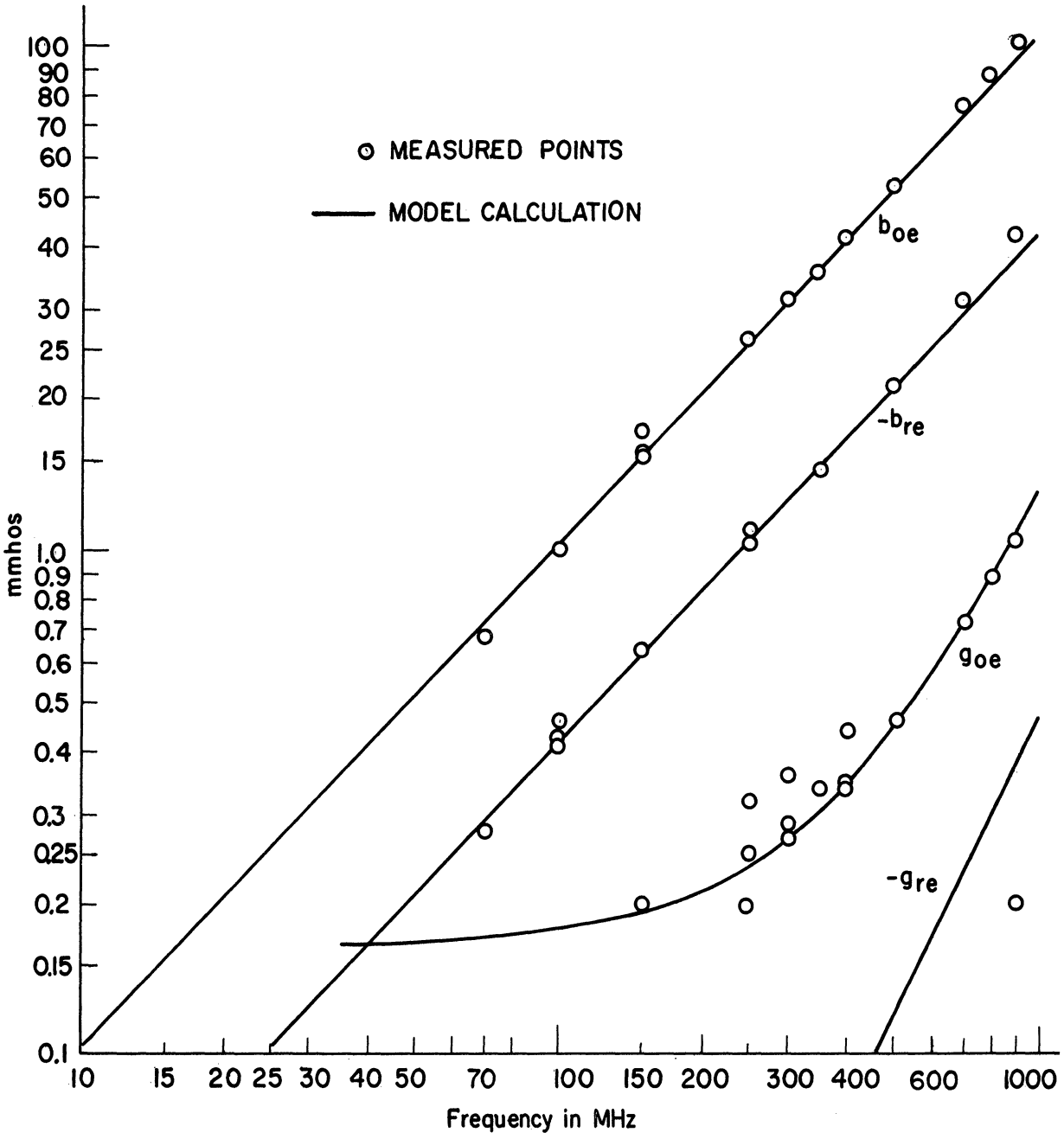

Fig. 7. Measured and calculated y_{oe} and y_{re} values for a 2N918 at 4 V and 2 mA

less than 0.068 pF (10 percent of the measured b_{re}), and for circuit design purposes it can be neglected.

For the conductance data, g_{re} was found to be too small for reliable measurement with the setup used. The measurement of g_{oe} is also difficult for this small transistor, and a number of additional measurements were made in an attempt to improve the data. Particularly at the lower frequencies, data spreads of up to ±30 percent are evident. Above 500 MHz, however, the data becomes reasonably smooth, and g_{oe} seems to approach an asymptotic slope of +2. At low frequencies, the data "appear" to approach a constant value between 0.15 and 0.2 millimhos.

The susceptance data are well-modeled by the circuit of Fig. 6(a), by making C_{BC} 0.68 pF and C_{CE} 0.95 pF. Adding a shunt resistor across C_{CE} with a value of 6000 ohms matches the low-frequency value of g_{oe}. The square-law frequency asymptote suggests a fixed resistance in series with the output capacity. For series RC circuit

$$Y_{\text{series RC}} = \frac{j\omega C}{1 + j\omega RC} \tag{14}$$

which reduces to

$$\approx \omega^2 C^2 R + j\omega C \tag{15}$$

as long as $\omega^2 R^2 C^2 << 1$.

In Fig. 7, g_{oe} at 900 MHz is 1.04 millimhos so that the series resistance should contribute 1.04 - 0.167 = 0.873 millimhos. Taking C as 1.63 pF one finds the needed series resistance is 10.4 ohms.

Figure 8(a) gives the one-, two-, and three-lump models optimized by the computer program to match the y_{ie} and y_{fe} data given in the appendix for the 2N918 at 4 V and 2 mA. Before carrying out the optimization the measured data (real and imaginary parts of the four y's) were plotted and "smoothed" by eye. The data fed into the optimization program were read from these smoothed curves at 15 frequencies spread relatively uniformly on a logarithmic frequency scale from 2 to 450 MHz.* With the weighting factors all taken as unity the mean square errors for these three models are 0.793, 0.107, and 0.0435. The improvement achieved by going from a one- to a two-lump model is significant; for circuit design purposes the additional improvement possible with three or more lumps seems less worthwhile for this transistor.

The models in Fig. 8(a) are for the input and forward characteristics only. Adding on $C_{BC'}$, $C_{CE'}$, $C_{BE'}$, and the output resistance to any of these circuits gives a complete model. This is illustrated in Fig. 8(b) for the two-lump case.

---

* That is, 2, 3, 4, 5, 7, 10, 15, 20, 45, ..., 450.

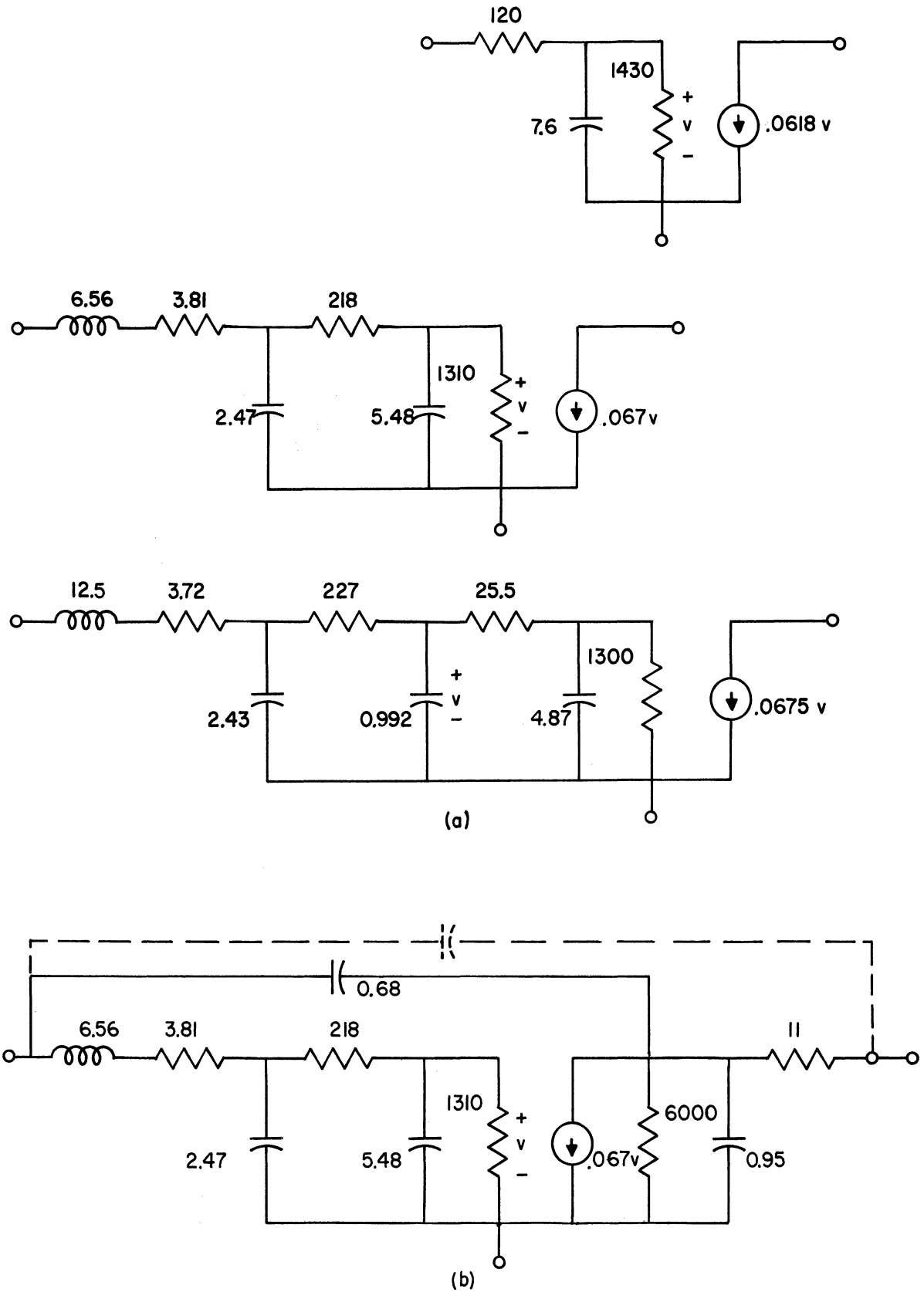

Fig. 8. (a) Computer optimized models for y_{ie} and y_{fe}
(b) A complete 2-lump model for 2N918 at $V_{ce} = 4V$, $I_c = 2mA$ (ohms, picafarad, nanohenrys, and mhos)

The nature of the model approximations is seen by examining the individual terms in Eq. 7. One hundred times these errors are plotted versus frequency in Fig. 9. For the one-lump (hybrid-pi) approximation, the y_{ie} error is less than 10 percent up to 95 MHz, but the y_{fe} error exceeds 10 percent above 28 MHz. The large difference in these two frequencies is in keeping with our observations in Section 1 of the inadequacy of the simple hybrid-pi for this transistor. With the two-lump model, the y_{ie} error is less than 10 percent up to 440 MHz, and the y_{fe} error reaches 10 percent at 325 MHz. The addition of just two elements allows a 3:1 improvement in the useable frequency range for the model and gives a much more balanced error. The addition of two more elements to make a three-lump approximation gives a further improvement particularly in y_{fe} above 50 MHz. Now the error magnitude never exceeds 7 percent over the full frequency range of 2 to 450 MHz.

The solid lines in Fig. 7 are calculated for the two-lump model of Fig. 8(b). The errors in b_{oe}, b_{re}, and g_{oe} are less than 10 percent out to 900 MHz. The calculated g_{re} is larger than our measurements indicated. (Our best estimate is that g_{re} is about -0.2 millimhos at 900 MHz.) For most circuit calculations this discrepency will not be significant since y_{re} is dominated by

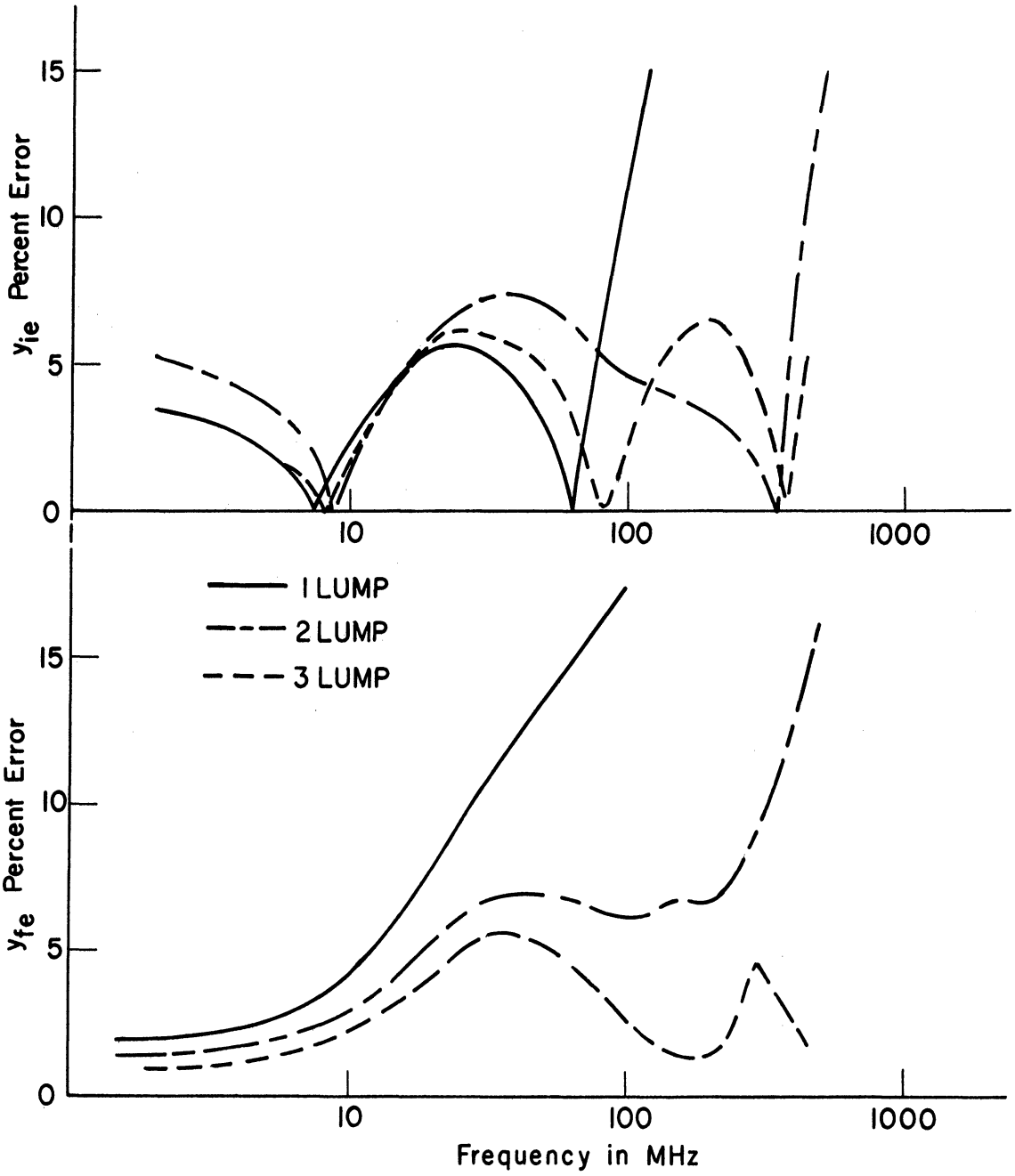

Fig. 9. Percentage error magnitude versus frequency for computer optimized 1-, 2-, and 3-lump models of a 2N918

b_{re}. If the refinement is desired, one can reduce the magnitude of g_{re} by splitting C_{BC} into two portions, one as shown, and a second directly between the base and collector external terminals as indicated by the dotted lines in Fig. 8(b).

The y_{ie} and y_{fe} admittance loci are plotted in Fig. 10 for the two-lump model of Fig. 8(b). The circled points are the input data for the computer optimization program.

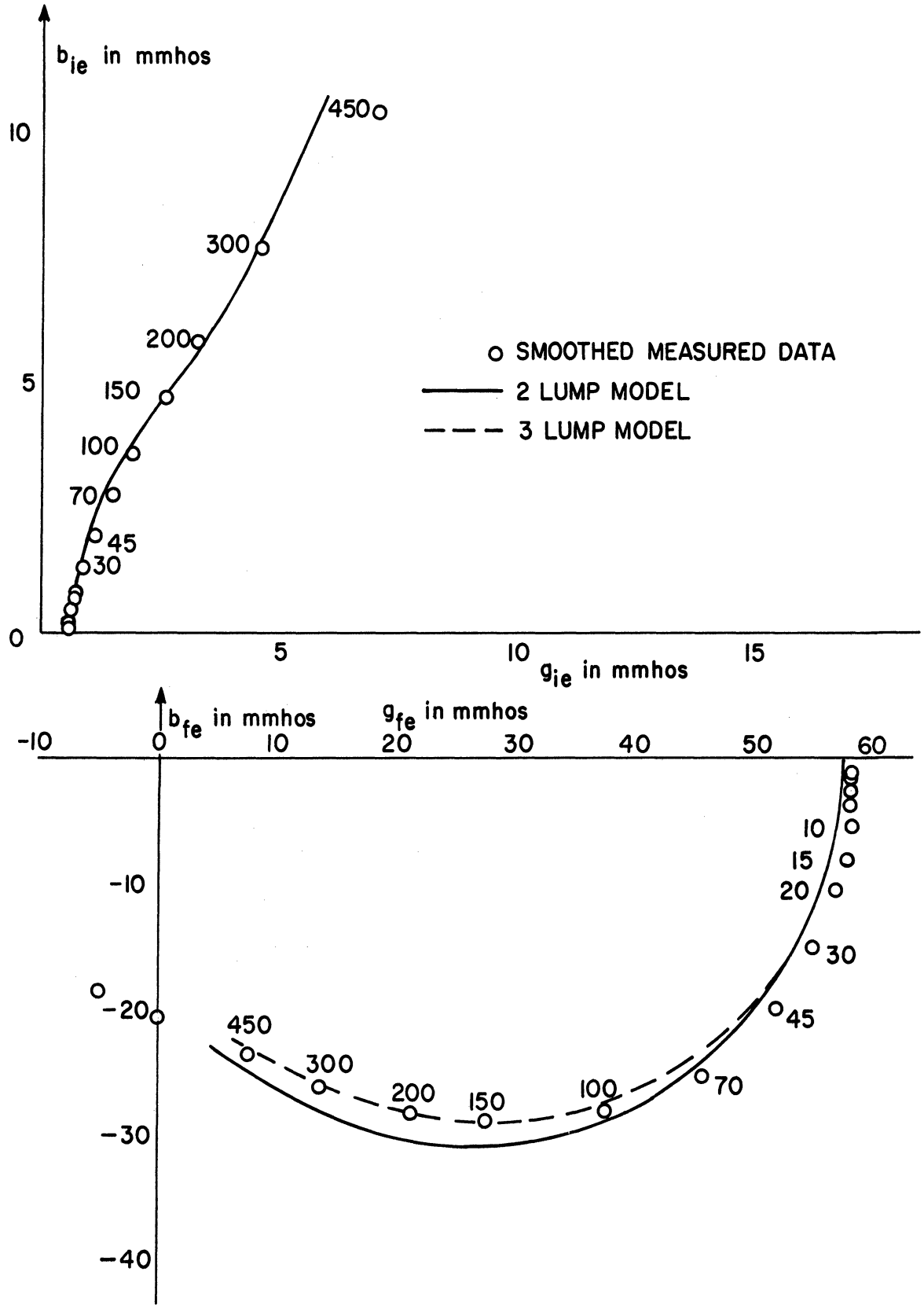

Fig. 10. Measured and calculated admittance loci for 2N918 at I_c = 2mA, V_{ce} = 4V; frequency is in megahertz

4. Typical Circuit Applications

The utility of one transistor model over another depends on the proposed application of the model. Since all models considered here are identical at low frequencies, we would expect that in low-pass circuits the differences in performance would be less than in bandpass circuits, particularly as the center frequencies exceed $f_T/10$ (about 90 MHz for the 2N918 example).

Two simple transistor amplifier circuits are shown in Fig. 11, an emitter-follower and a simple, single-tuned amplifier. The emitter-follower with a 1000 ohm resistive source and a parallel RC load of 100 ohms and 30 pF is a low-pass circuit with a -3dB bandwidth of the order of 100 MHz. In the second circuit the output inductors transform the 50-ohm load to match y_{oe} at 225 MHz, and the input simply cancels the input susceptance at the same frequency. The overall frequency response is essentially that of the output single-tuned circuit.

Both of the circuits in Fig. 11 were analyzed using a linear circuit analysis program that calculated the poles and zeros of the specified input-output pairs as well as frequency and time responses. Table I summarizes the calculated poles and zeros, the frequency response, and the step response characteristics of the emitter-follower circuit. The step responses are plotted in Fig. 12. There are clear

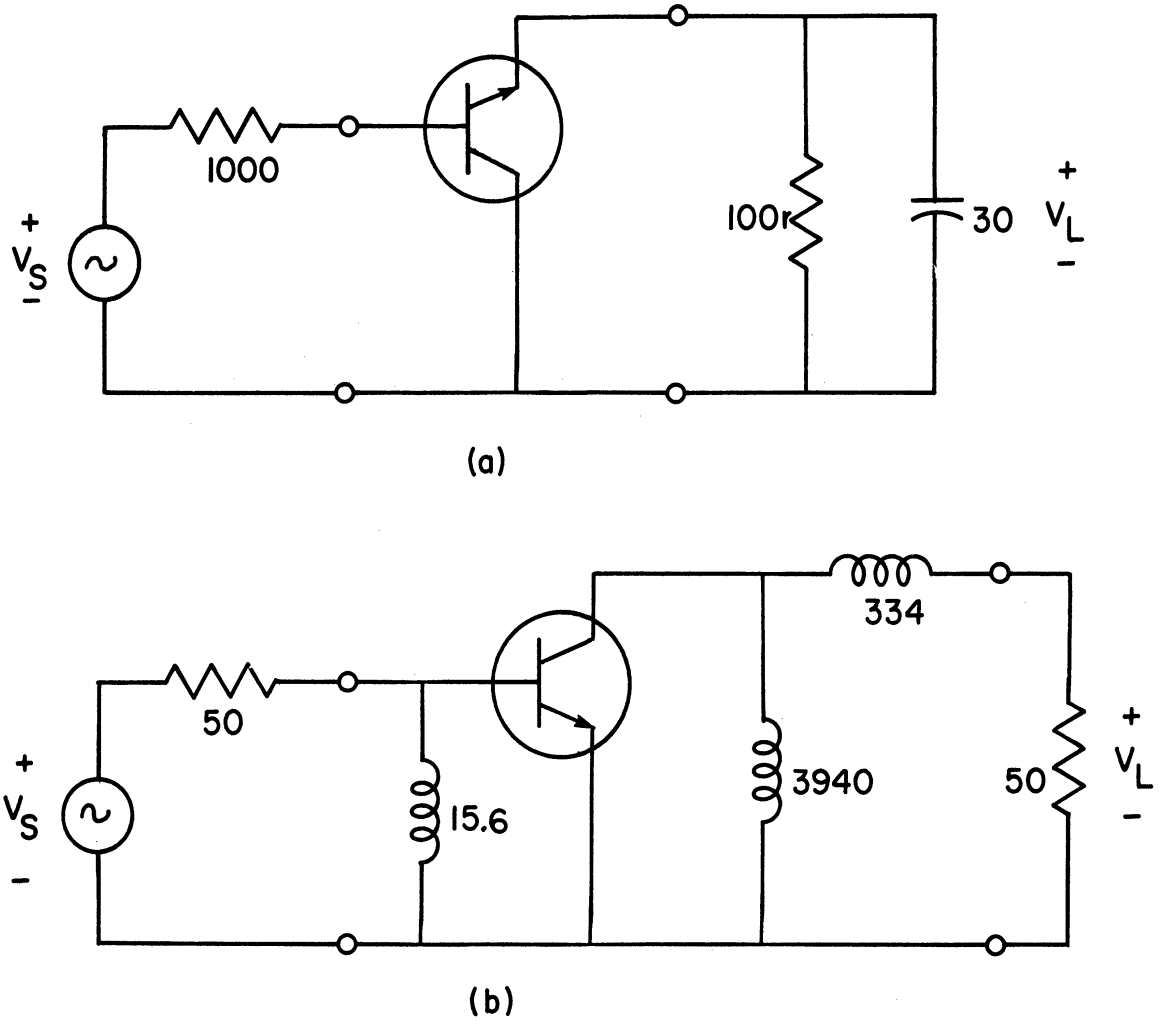

Fig. 11. Typical circuits for comparing transistor models; (a) emitter-follower (b) 200 MHz tuned amplifier, (ohms, picofarads, nanohenrys)

Calculated Characteristics	Transistor Model Used [Fig. 8(a)]		
	hybrid-pi	2-lump	3-lump
Poles (Gigarad)	-109.3 - 14.07 -.3319±j.3994	-98.41 -1.787±j17.02 -.3078±j.4334 -2.603	-99.15 -51.56 -1.231±j12.36 -.3063±j.4225 -2.305
Zeros (Gigarad)	-6.928±j32.89 -8.533	-11.03±j28.48 -23.09 -1.276±j4.608	-51.59 9.854±j22.05 -18.05 -2.265±j4.011
Voltage Gain	-2.187 dB	-2.179 dB	-2.162 dB
Bandwidth (-3dB)	90 MHz	95.5 MHz	93.5 MHz
Gain Peak	-2.067 dB at 31.6 MHz	-1.813 dB at 42.2 MHz	-1.836 dB at 42.2 MHz
Rise Time in ns (10-90%)	3.78	3.54	3.58
Delay Time	2.64	2.80	2.80
Overshoot	7.5%	10.4%	10.2%

Table I. Model comparison in emitter follower circuit

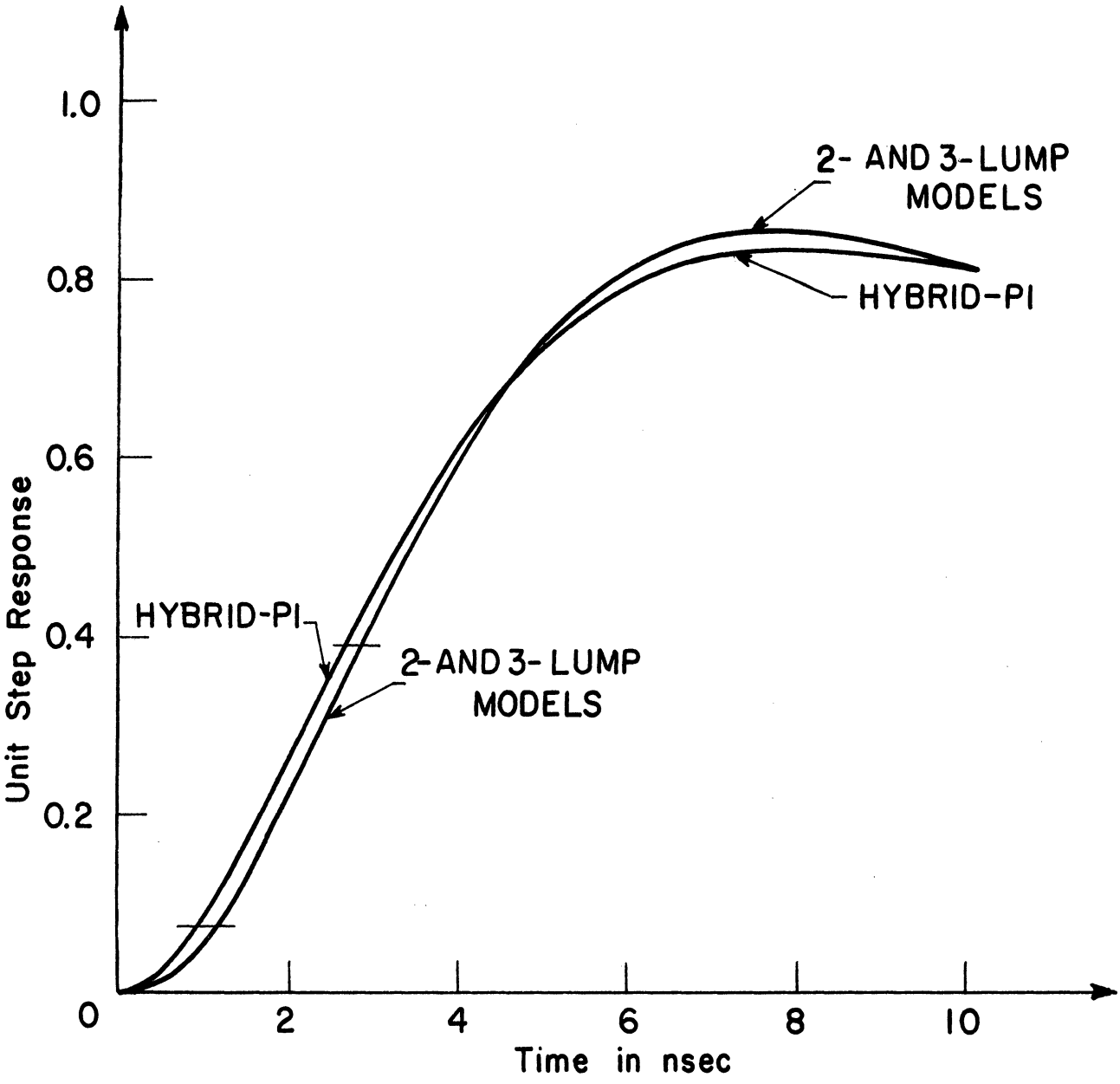

Fig. 12. Calculated emitter follower step responses using 1-, 2-, and 3-lump 2N918 models

differences between the responses calculated with the hybrid-pi and those calculated using either the two- or three-lump model; the larger models predict more overshoot and delay and shorter rise-times. These differences are all small, and those between the two- and three-lump models are certainly negligible in this circuit.

Table II summarizes calculated performance of the tuned amplifier. As in the emitter-follower example, there is a significant change when the hybrid-pi is replaced by the two- or three-lump model but the difference between the performance with the last two is much smaller. The three, calculated frequency response curves are given in Fig. 13. In this example, the small difference between the two- and three-lump models is attributable in part to the circuit design, which makes the relatively unchanging output admittance the most important frequency determining element. In some bandpass designs we have observed significant differences between the predictions of the two larger models.

Calculated Characteristic	Transistor Model Used [Fig. 8(a)]		
	hybrid-pi	2-lump	3-lump
Poles (gigarad)	-68.5 -3.27 -1.14 -0.0116 -.0792±j1.23	-35.3 -10.9 -0.933 -0.0116 -.0981±j1.23 -3.44±j4.93	-51.0 -5.77 -0.830 -0.0116 -0.978±j1.24 -2.36±j4.80 -42.5
Zeros (gigarad)	-10.6 9.41 0. 0.	-0.993±j10.3 6.19 -7.62 0. 0.	-51.6 -1.95±j8.39 6.21 -5.02 0. 0.
Maximum T.P.G.	20.0 dB	17.8 dB	17.4 dB
Center Frequency	195 MHz	195 MHz	197 MHz
Bandwidth (-3dB)	25.5 MHz	31.6 MHz	31 MHz

Table II. Model comparison in tuned amplifier

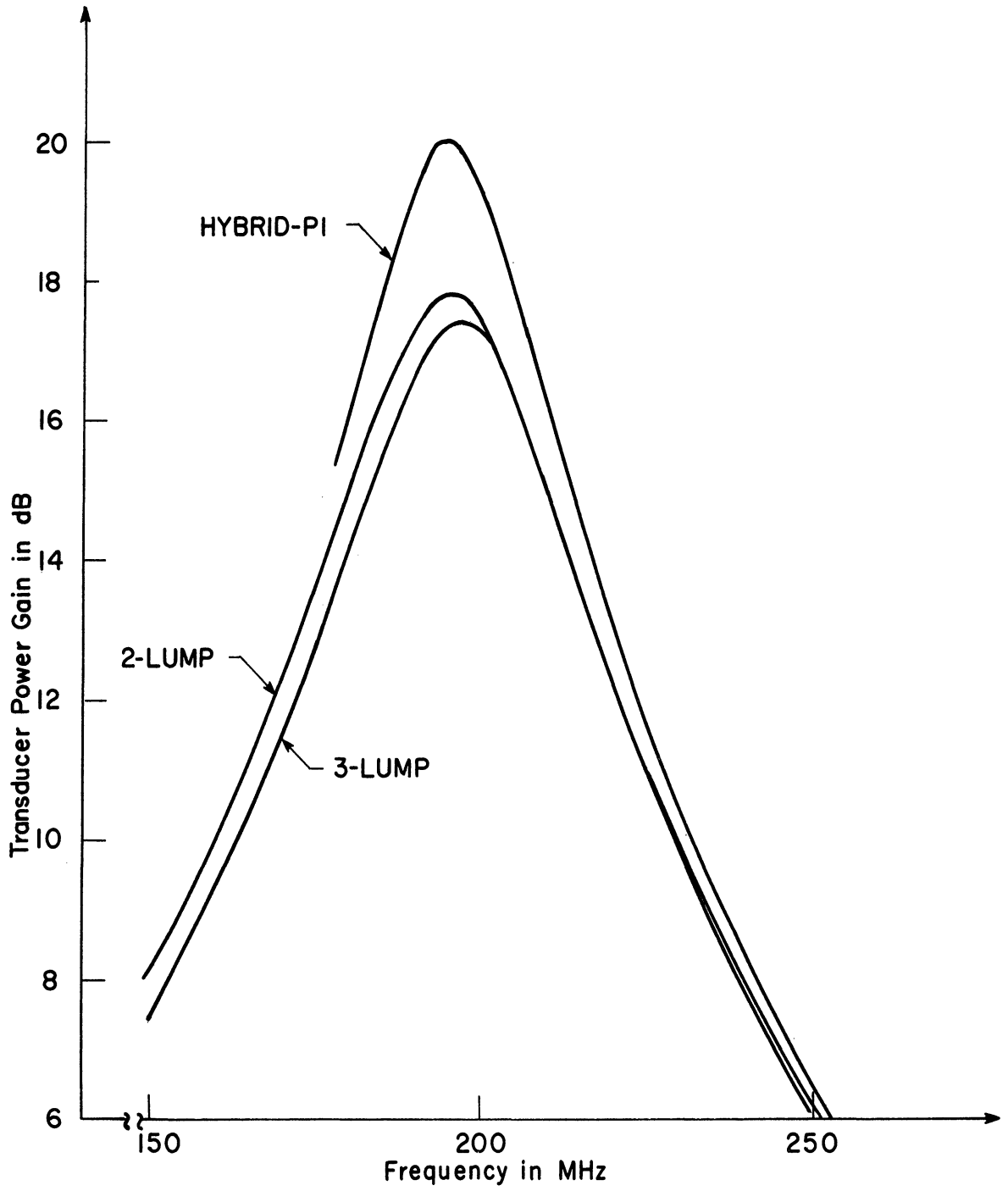

Fig. 13. Calculated frequency response of 200 MHz amplifier using 1-, 2-, and 3-lump 2N918 models

5. Conclusions

At the outset it was pointed out that the hybrid-pi circuit plus extrinsic elements cannot accurately model certain small transistors over wide frequency ranges. The suitability of the hybrid-pi model for a given transistor is established easily with the y_{ie} and y_{fe} admittance loci. The hybrid model can be expected to be satisfactory if the susceptance maxima of these two admittances occur at about the same frequency. We have examined the admittance data compiled by Sidney C. Chao for 16 transistor types (Ref. 3). For 14 of these we plotted Chao's data and observed or estimated the frequency of the susceptance maxima.* Table III summarizes the results of these observations. If the ratio of the frequencies at which the susceptance maxima occurs is 1.5 or less, it seems probable that a one-lump or hybrid-pi model will be satisfactory. When the ratio exceeds 1.5, it is expected that a multilump model will be required to match the transistor characteristics closely over a wide frequency range. On this basis, five of the transistors listed in Table III would require a multilump model: the 2N918, 2N2219, 2N2708, 2N2929, and 2N3663. It is not obvious to the writers, from published information, what makes these five types electrically so different from the other members of the table.

* The two transistors omitted were both experimental units.

Transistor	Quiescent point V_{CE} in volt I_c in mA		Frequency of susceptance maxima in MHz		Frequency ratio
			y_{ie}	y_{fe}	
2N918	4	2.0	750	150	5.0
2N2219	20	20.0	150	<50	>3.0
2N2415	6	2.0	300	300	1.0
2N2708	15	2.0	600	50	12.0
2N2857	6	1.5	500	300	1.7
2N2865	10	4.0	400	300	1.3
2N2929	-10	-10.0	100	40	2.5
2N3282	-10	- 3.0	300	200	1.5
2N3553	28	25.0	29	33	0.88
2N3570	10	5.0	400	400	1.0
2N3662	10	5.0	450	120	3.7
2N3688	10	4.0	150	100	1.5
2N3783	-10	-3.0	200	200	1.0
2N3866	15	10.0	130	150	0.87

Table III. Frequencies of susceptance maxima for typical transistors

From the circuit designer's viewpoint, the why of the need for a distributed, stored-charge model is less important than the fact that such a model may be needed if certain transistor types are to be employed. If the transistor manufacturer furnishes typical data that establishes the y-parameters as a function of frequency, it is a simple matter to determine whether a multilump model should be considered.

If not, the measurement of y_{ie} and y_{fe} versus frequency at a single quiescent point should be sufficient to establish the frequency ratio of Table III. Finally, if one wishes to play probabilities, our investigation of Chao's data suggests that there is at least a 60 percent probability that the simple hybrid-pi will be adequate.

A two-lump extension of the hybrid-pi model does not represent a great increase in circuit complexity, particularly when computer analysis programs are used. This is particularly true since in the frequency ranges where these effects are noticeable, some of the extrinsic transistor parameters are almost certain to be important. The multilump models can match the transistor characteristics over the complete frequency range 0 to about f_T. When only a limited frequency interval is of interest, a simple hybrid-pi model can be optimized for a particular frequency range, such as $0.4\ f_T$ to $0.5\ f_T$, even though a multilump model might be required for the full range, 0 to $0.5\ f_T$. In this connection, it should be noted that an approximate "excess phase" can be added easily to the usual hybrid-pi model by paralleling the g_m-generator with a second current generator flowing from emitter to collector and controlled by the current in the C_π capacity (Ref. 8).

REFERENCES

1. R. L. Pritchard, Electrical Characteristics of Transistors, McGraw-Hill, 1967, Chapters 5 and 6; contains a very complete bibliography.

2. P. E. Gray, et al., Physical Electronics and Circuit Models of Transistors, SEEC, Vol. 2, John Wiley & Sons, 1969, Chapter 8.

3. Sidney C. Chao, Application of Computers to RF Circuit Design, Final Report on Contract DA28-043 AMC-01347(E), ECOM-01347-F, June 1966.

4. Fairchild Semiconductor Transistor and Diode Data Catalog 1970, pp. 2-66.

5. J. L. Herrero and G. Willoner, Synthesis of Filters, Prentice-Hall, 1966, Chapter 1.

6. D. A. Calahan, Computer-aided Network Design, Preliminary Edition, McGraw-Hill, 1968, pp. 289-293.

7. IBM System/360 Scientific Subroutine Package, FMFP and FMCG, H20-0205-2, pp. 202-206.

8. Semiconductor Circuits, Engineering Summer Conference Course 7007, University of Michigan, Ann Arbor, June 1-5, 1970, Chapter 12.

APPENDIX A

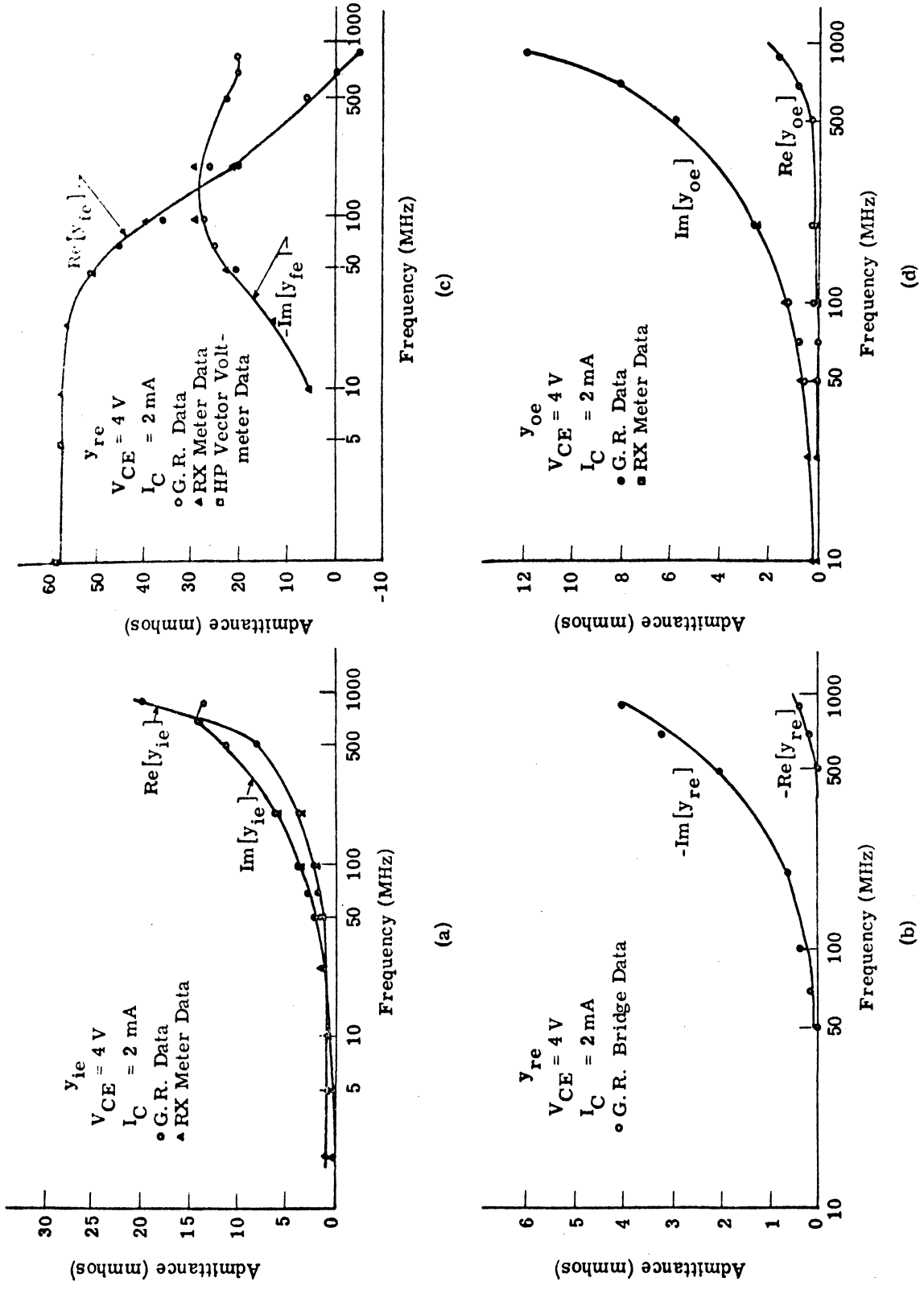

Fig. 14. Plots of measured y parameters for 2N918: (a) y_{ie} (b) y_{re} (c) y_{fe} (d) y_{oe}

	Frequency (MHz)	V_{CE} = 4 V I_C = .5 mA	V_{CE} = 4 V I_C = 1 mA	V_{CE} = 4 V I_C = 2 mA	V_{CE} = 4 V I_C = 4 mA	V_{CE} = 4 V I_C = 8 mA	V_{CE} = 1 V I_C = 2 mA	V_{CE} = 2 V I_C = 2 mA	V_{CE} = 8 V I_C = 2 mA
(a) y_{ie} in millimhos	50	0.6 + j 1.6	0.6 + j 1.6	1.2 + j 2.2	2.0 + j 3.0	3.4 + j 3.4	1.4 + j 2.6	1.4 + j 2.6	1.4 + j 2.6
	70	0.4 + j 2.2	1.0 + j 2.4	1.6 + j 3.0	2.6 + j 3.6	4.0 + j 4.4	1.6 + j 3.2	1.6 + j 3.2	1.4 + j 2.8
	100	0.8 + j 2.8	1.4 + j 3.2	2.2 + j 3.6	3.4 + j 4.4	5.0 + j 6.8	2.4 + j 4.0	2.4 + j 3.8	2.0 + j 3.4
	200	2.0 + j 5.0	2.8 + j 5.6	3.8 + j 6.0	5.4 + j 6.4	7.8 + j 8.0	4.2 + j 6.6	4.0 + j 6.2	3.4 + j 5.8
	500	4.4 + j 9.8	5.8 + j10.2	7.8 + j11.0	11.2 + j11.4	16.0 + j10.8	8.8 + j12.2	8.4 + j10.6	7.2 + j10.6
	700	8.4 + j13.8	10.6 + j14.2	13.8 + j14.0	18.2 + j12.4	23.0 + j11.0	15.6 + j15.6	14.8 + j14.6	12.6 + j15.8
	900	12.6 + j16.0	15.8 + j15.6	19.8 + j13.4	23.4 + j 8.7	25.5 + j 2.7	22.1 + j14.7	21.3 + j14.4	18.6 + j13.5
	Frequency (MHz)	V_{CE} = 4 V I_C = .5 mA	V_{CE} = 4 V I_C = 1 mA	V_{CE} = 4 V I_C = 2 mA	V_{CE} = 4 V I_C = 4 mA	V_{CE} = 4 V I_C = 8 mA	V_{CE} = 1 V I_C = 2 mA	V_{CE} = 2 V I_C = 2 mA	V_{CE} = 8 V I_C = 2 mA
(b) y_{oe} in millimhos	50	j 0.6	j 0.6	j 0.6	j 0.6	j 0.6	j 0.6	j 0.6	j 0.6
	70	j 0.8	j 0.8	j 0.8	j 0.8	j 0.8	j 0.8	j 0.8	j 0.8
	100	0.2 + j 1.2	0.2 + j 1.2	0.2 + j 1.2	0.2 + j 1.2	0.2 + j 1.2	0.2 + j 1.6	0.2 + j 1.4	0.2 + j 1.2
	200	0.2 + j 2.6	0.2 + j 2.6	0.2 + j 2.6	0.2 + j 2.6	0.2 + j 2.6	0.2 + j 3.0	0.2 + j 3.0	0.2 + j 2.4
	500	0.4 + j 6.0	0.4 + j 6.0	0.4 + j 6.2	0.3 + j 6.2	0.8 + j 6.2	1.0 + j 7.2	0.8 + j 6.6	0.6 + j 5.8
	700	0.6 + j 8.4	0.8 + j 8.4	1.0 + j 8.4	1.0 + j 8.4	1.2 + j 8.4	1.6 + j10.2	1.2 + j 9.0	0.8 + j 7.8
	900	1.2 + j12.4	1.4 + j12.2	1.8 + j12.2	2.0 + j12.0	2.2 + j11.8	3.2 + j15.0	2.2 + j12.8	1.4 + j11.0

	Frequency (MHz)	V_{CE} = 4 V I_C = .5 mA	V_{CE} = 4 V I_C = 1 mA	V_{CE} = 4 V I_C = 2 mA	V_{CE} = 4 V I_C = 4 mA	V_{CE} = 4 V I_C = 8 mA	V_{CE} = 1 V I_C = 2 mA	V_{CE} = 2 V I_C = 2 mA	V_{CE} = 8 V I_C = 2 mA
(c) y_{fe} in millimhos	50	18.4 - j 3.8	31.2 - j 8.7	52.0 - j20.4	73.8 - j40.8	93.0 - j67.0	52.0 - j21.6	52.8 - j20.8	51.0 - j20.4
	70	17.4 - j 4.8	29.0 - j10.8	45.6 - j24.8	61.2 - j44.4	70.8 - j66.6	44.4 - j18.0	44.4 - j23.4	45.6 - j24.6
	100	15.6 - j 6.4	25.2 - j13.4	36.6 - j26.1	45.2 - j42.8	50.4 - j57.6	34.2 - j25.2	35.4 - j25.8	35.4 - j25.5
	200	11.0 - j 8.8	16.0 - j16.0	20.6 - j26.2	24.0 - j37.2	25.2 - j49.2	20.0 - j27.6	20.6 - j26.8	20.2 - j25.2
	500	4.6 - j10.8	5.6 - j16.0	6.0 - j22.0	3.6 - j30.3	-1.5 - j36.9	5.4 - j23.1	5.6 - j23.0	6.4 - j21.6
	700	1.8 - j10.0	1.8 - j14.4	- j20.6	-4.4 - j26.8	-11.6 - j29.4	1.4 - j22.4	0.2 - j21.6	-0.8 - j20.0
	900	0.4 - j10.4	-0.2 - j14.4	-5.0 - j20.4	-12.4 - j23.4	-18.0 - j21.0	-8.0 - j22.4	-6.4 - j21.4	-3.2 - j19.4
	Frequency (MHz)	V_{CE} = 4 V I_C = .5 mA	V_{CE} = 4 V I_C = 1 mA	V_{CE} = 4 V I_C = 2 mA	V_{CE} = 4 V I_C = 4 mA	V_{CE} = 4 V I_C = 8 mA	V_{CE} = 1 V I_C = 2 mA	V_{CE} = 2 V I_C = 2 mA	V_{CE} = 8 V I_C = 2 mA
(d) y_{re} in millimhos	50	0	0	0	0	0	0	0	0
	70	- j 0.2	- j 0.2	- j 0.2	- j 0.2	- j 0.2	- j 0.2	- j 0.2	- j 0.2
	100	- j 0.4	- j 0.4	- j 0.4	- j 0.4	- j 0.4	- j 0.4	- j 0.4	- j 0.4
	200	- j 0.8	- j 0.6	- j 0.6	- j 0.6	- j 0.6	- j 1.0	- j 0.8	- j 0.6
	500	- j 2.0	- j 2.0	- j 2.0	- j 2.0	- j 2.0	- j 3.2	- j 2.4	- j 1.8
	700	-0.2 - j 3.2	-0.2 - j 3.2	-0.2 - j 3.2	-0.2 - j 3.2	-0.2 - j 3.2	-0.4 - j 4.4	-0.2 - j 3.8	- j 2.4
	900	-0.4 - j 4.0	-0.4 - j 4.0	-0.4 - j 4.0	-0.4 - j 3.8	-0.4 - j 3.8	-1.8 - j 5.8	-1.0 - j 4.6	-0.2 - j 3.2

Table IV. Short circuit admittance parameters of a 2N918 transistor measured on G. R. Transfer function and Immittance Bridge

Frequency (MHz)	V_{CE} = 4 V I_C = .5 mA	V_{CE} = 4 V I_C = 1 mA	V_{CE} = 4 V I_C = 2 mA	V_{CE} = 4 V I_C = 4 mA	V_{CE} = 4 V I_C = 8 mA	V_{CE} = 1 V I_C = 2 mA	V_{CE} = 2 V I_C = 2 mA	V_{CE} = 8 V I_C = 2 mA
50	2.20 - j 9.40	3.10 - j13.50	3.60 - j16.60	3.60 - j19.20	3.20 - j19.00	2.80 - j14.80	3.20 - j15.60	3.60 - j16.80
70	0.30 - j 7.25	0.50 - j10.20	0.50 - j13.40	0.40 - j14.20	0.20 - j13.80	0.20 - j12.30	0.40 - j13.00	0.40 - j14.20
100	-0.40 - j 5.15	-0.60 - j07.20	-0.90 - j 9.30	-1.20 - j10.40	-1.30 - j10.10	-0.90 - j 8.40	-0.80 - j 8.90	-0.90 - j 9.70
200	-0.78 - j 2.46	-1.11 - j 3.45	-1.44 - j 4.26	-1.60 - j 4.70	-1.50 - j 4.60	-1.45 - j 3.85	-1.50 - j 4.15	-1.55 - j 4.40
500	-0.55 - j 0.82	-0.73 - j 1.08	-0.88 - j 1.33	-0.96 - j 1.52	-0.93 - j 1.50	-0.90 - j 1.23	-0.89 - j 1.29	-0.90 - j 1.38
700	-0.43 - j 0.38	-0.58 - j 0.58	-0.72 - j 0.78	-0.81 - j 0.94	-0.80 - j 0.98	-0.75 - j 0.63	-0.74 - j 0.77	-0.72 - j 0.79
900	-0.40 j 0.32	-0.51 - j 0.45	-0.67 - j 0.61	-0.78 - j 0.70	-0.77 - j 0.74	-0.62 - j 0.56	-0.67 - j 0.59	-0.67 - j 0.60

Table V. Short circuit current gain of a 2N918 transistor measured on G. R. Transfer-Function Bridge

Frequency (MHz)	V_{CE} = 4 V I_C = .5 mA	V_{CE} = 4 V I_C = 1 mA	V_{CE} = 4 V I_C = 2 mA	V_{CE} = 4 V I_C = 4 mA	V_{CE} = 4 V I_C = 8 mA	V_{CE} = 1 V I_C = 2 mA	V_{CE} = 2 V I_C = 2 mA	V_{CE} = 8 V I_C = 2 mA
2	0.21 + j0.04	0.38 + j0.07	0.62 + j0.08	1.1i + j0.12	1.89 + j0.16	0.68 + j0.10	0.65 + j0.10	0.57 + j0.09
5	0.22 + j0.16	0.40 + j0.20	0.64 + j0.25	1.15 + j0.36	1.96 + j0.59	0.68 + j0.27	0.66 + j0.26	0.58 + j0.25
10	0.24 + j0.30	0.43 + j0.39	0.67 + j0.47	1.19 + j0.64	2.13 + j0.90	0.74 + j0.52	0.70 + j0.50	0.59 + j0.44
25	0.26 + j0.71	0.49 + j0.91	0.83 + j1.15	1.42 + j1.43	2.55 + j1.91	0.87 + j1.24	0.80 + j1.16	0.67 + j1.04
50	0.33 + j1.41	0.64 + j1.72	1.12 + j2.06	2.01 + j2.50	3.39 + j2.87	1.33 + j2.37	1.20 + j2.16	0.99 + j1.89
100	0.64 + j2.63	1.23 + j2.97	1.96 + j3.29	2.94 + j3.62	4.52 + j4.11	2.10 + j3.65	2.00 + j3.41	1.72 + j3.13
200	1.77 + j4.77	2.58 + j5.15	3.32 + j5.76	4.60 + j6.33	7.39 + j7.22	3.60 + j6.43	3.31 + j5.86	3.06 + j5.30

(a) y_{ie} in millimhos

Frequency (MHz)	y_{oe} (mmhos)	y_{ib} (mmhos)	y_{fe} (mmhos)
10	0.01 + j 0.14	59.26 - j 4.74	58.58 - j 5.35
25	0.01 + j 0.33	58.00 - j11.24	57.16 - j12.72
50	0.06 + j 0.66	52.57 - j19.97	51.39 - j22.69
100	0.12 + j 1.31	42.53 - j24.54	40.44 - j29.13
200	0.09 + j 2.44	25.11 - j21.33	21.70 - j29.52

(b) y_{oe}, y_{ib}, and calculated y_{fe} at V_{CE} = 4 V, I_C = 2 mA

Table VI. Short circuit admittance parameters of a 2N918 measured with RX meter and a Transistor Test Jig

```
C*****THIS PROGRAM MAY BE USED TO IMPROVE THE VECTOR DIFFERENCE FOR BOTH
C      Y11 AND Y21 BETWEEN THE DESIRED RESPONSE AND THE ACTUAL RESPONSE
C      FOR THE LADDER TYPE TWO LUMP TRANSISTOR MODEL.
C
       COMPLEX FCTN1(20),FCTN2(20),S,JAY/(0.0,1.0)/,A(20)/20*(0.0,0.0)/
       COMPLEX CUMUL,DEN,B(20)/20*(0.0,0.0)/,Y11,Y21
       DIMENSION AA(20),FREQ(20),G(20)
       INTEGER P, BRANCH
       JUMP=0
       ITER=0
C
C      READ NUMBER OF ELEMENTS--N,N=NUMBER OF LADDER ELEMENTS + 1
C       P=POWER TO WHICH ERROR-CRITERION IS RAISED
C       BRANCH=THE CURRENT GENERATOR'S CONTROLLING BRANCH NUMBER
       READ(5,2) N,BRANCH,P
2      FORMAT(3I2)
       NM=N-1
       NN=N-3
       NT=N+1
C
C      READ ELEMENT VALUES AA(1)...AA(N),  AA(N) IS GM, AA(N+1) IS LB
C      NETWORK IS FREQUENCY SCALED BY 10**-9
C      NETWORK IS MAGNITUDE SCALED BY 10**-3
       READ(5,1) (AA(J),J=1,NT)
 1     FORMAT(6F10.0)
C      READ DESIRED RESPONSE DATA
       READ(5,3) NFREQ, (FREQ(J),FCTN1(J),FCTN2(J),J=1,NFREQ)
3      FORMAT(I2/(5F10.0))
       READ(5,160) CBE,CBC,WY11,WY21
160    FORMAT(4F10.0)
       WRITE(6,165) CBE,CBC,WY11,WY21
165    FORMAT(//,10X,4HCBE=,F8.4,10X,4HCBC=,F8.4/10X,5HWY11=,F8.4,9X,
      15HWY21=,F8.4)
       DO 170 I=1,NFREQ
       FCTN1(I)=FCTN1(I)-JAY*6.2831854*FREQ(I)*(CBE+CBC)
170    FCTN2(I)=FCTN2(I)+JAY*6.2831854*FREQ(I)*CBC
```

```
      100   WRITE(6,4)  (AA(J),J=1,NT)
    4       FORMAT(//,10X,23HTHE MODEL ELEMENTS ARE  ,//(6F10.5))
            ALFSAV=.000001
            IF(ITER)19,20,19
     19     STOP
    C
    20      CALL MIN(ERR,G,AA,NT,.99,JUMP,NT,ALFSAV,2.,1)
            IJ=ITER*JUMP
            ERR=0.
            IF(IJ)8,7,8
    7       WRITE(6,6)
    6       FORMAT(///3X,4HFREQ,5X,7HRE(Y11),3X,7HIM(Y11),3X,7HRE(Y21),3X,
           17HIM(Y21),3X,6HERRY11,4X,6HERRY21,/3X,5H(GHZ),4X,6H(MMHO),4X,
           26H(MMHO),4X,6H(MMHO),4X,6H(MMHO),4X,6H(MMHO),4X,6H(MMHO),/)
    8       DO 9 J=1,NFREQ
            S=JAY*FREQ(J)*6.2831854
            DO 90 K=1,NN,2
            A(K)=AA(K)
    90      A(K+1)=S*AA(K+1)
            A(1)=A(1)+S*AA(NT)
            A(NM)=AA(NM)
            DEN=CUMUL(A,NM)
            Y11=CUMUL(A(2),NM-1)/DEN
            Y21=AA(N)*CUMUL(A(BRANCH+1),NM-BRANCH)/DEN
            ERRY11=CABS(FCTN1(J)-Y11)/CABS(FCTN1(J))
            ERRY21=CABS(FCTN2(J)-Y21)/CABS(FCTN2(J))
            IF(IJ)9,11,9
    11      Y11=Y11+S*(CBC+CBE)
            Y21=Y21-S*CBC
            WRITE(6,10) FREQ(J),Y11,Y21,ERRY11,ERRY21
    10      FORMAT(7F10.4)
            IF(J-NFREQ)9,53,9
    53      WRITE(6,55)
     55       FORMAT(//,27HTHE MEAN SQUARE ERRORS ARE     /)
    9       ERR=ERR+(WY11*ERRY11)**P+(WY21*ERRY21)**P
    C
```

```
   73              WRITE(6,29) ERR
   74           29  FORMAT(F15.7)
   75              IF(JUMP)20,100,24
   76         C
   77         C    CALCULATE THE GRADIENTS
   78         24   DO 14 J=1,NT
   79              AASAV=AA(J)*.0001
   80              AA(J)=AA(J)+AASAV
   81              ERR1=0.
   82              DO 17 K=1,NFREQ
   83              S=JAY*FREQ(K)*6.2831854
   84              DO 99 I=1,NN,2
   85              A(I)=AA(I)
   86         99   A(I+1)=S*AA(I+1)
   87              A(1)=A(1)+S*AA(NT)
   88              A(NM)=AA(NM)
   89              DEN=CUMUL(A,NM)
   90              Y11=CUMUL(A(2),NM-1)/DEN
   91              Y21=AA(N)*CUMUL(A(BRANCH+1),NM-BRANCH)/DEN
   92         17   ERR1=ERR1+(WY11*CABS(FCTN1(K)-Y11)/CABS(FCTN1(K)))**P
   93             1+(WY21*CABS(FCTN2(K)-Y21)/CABS(FCTN2(K)))**P
   94              IF (ABS(ERR1-ERR).GE..0001.OR.ABS(AA(J)).GE..001) GO TO 300
   95              G(J)=1.0E-10
   96              GO TO 301
   97         300  G(J)=(ERR1-ERR)/AASAV
   98         301  CONTINUE
   99              AA(J)=AA(J)-AASAV
  100              WRITE (6,200) G(J),AA(J)
  101         200  FORMAT(10X,F15.7,5X,F10.5)
  102         14   CONTINUE
  103         C
  104              ITER=ITER+1
  105              GO TO 20
  106              END
ND OF FILE
```

```
      1              COMPLEX FUNCTION CUMUL(B,N)
      2        C
      3              COMPLEX B(20),C,OLDC,NEWC
      4              I=0
      5              C=1.
      6              OLDC=0.
      7        6     I=I+1
      8              NEWC=C*B(I)+OLDC
      9              OLDC=C
     10              C=NEWC
     11              IF(I-N)6,11,11
     12        11    CUMUL=C
     13              END
     14        C
     15        C
END OF FILE
```



```
$COPY FROM *SOURCE* TO -MIN
$LIST -MIN
      1              SUBROUTINE MIN(F,G,X,N,ERRCR,JUMP,NITER,ALFSAV,ALFMUL,NPRINT)
      2              DIMENSION G(20),X(20),GSAVE(20),S(20),SIG(20),DG(20), H(20,20),
      3             1A(20,20),B(20,20),C(20,20),XSAVE(20)
      4        C*****THIS SUBROUTINE MINIMIZES A FUNCTION F
      5        C     USING FLETCHER-POWELL WITH A SEARCH TO FIND MIN
      6        C     X(J) IS VARIABLE,G(J) IS GRADIENT,F IS FUNCTION
      7        C     JUMP=0 AT START AND FINISH OF ITERATION
      8        C     JUMP=1 REQUIRES CALCULATION OF FUNCTION AND GRADIENT
      9              IF(JUMP)20,1,20
     10        1     KEY=1
     11              JUMP=1
     12              RETURN
     13         20   GO TO(18,17,36,38,38,38,19),KEY
     14         18   FSAVE=F
     15              ITER=NITER
```

```
16              DO 14 J=1,N
17              XSAVE(J)=X(J)
18        14    GSAVE(J)=G(J)
19        34    I=0
20              IMAX=1
21              KEY=2
22              F1=FSAVE
23              F2=FSAVE
24              X1=0.
25              X2=0.
26              IF(JUMP)58,58,56
27        56    DO 12 J=1,N
28              DO 13 K=1,N
29        13    H(J,K)=0.
30        12    H(J,J)=1.
31              NGRAD=0
32              JUMP=-1
33        58    CALL MATMUL(H,N,N,G,1,S,-1.,20,1,20)
34              CALL MATMUL(S,1,N,G,1,DEM,1.,1,1,1)
35              IF(DEM)5,56,56
36        5     ALF=ALFSAV
37              ALFSAV=0.
38              GO TO 15
39        C     HAS MINIMUM BEEN BOUNDED
40        17    IF(F)44,44,31
41        44    ALFSAV=ALFSAV-ALF
42              ALF=ALF/ALFMUL**4
43              GO TO 15
44        31    IF((F-F2)/F-.000001)28,28,3
45        C     DECREASE SEARCH STEP SIZE IF ON FIRST ITERATION
46        3     GO TO (4,30),IMAX
47        4     ALFSAV=ALFSAV/(ALFMUL)**2
48              GO TO 5
49        C     MINIMUM NOT BOUNDED,DOUBLE STEP SIZE
50        28    F1=F2
51              F2=F
```

```
52              X1=X2
53              X2=ALFSAV
54              IMAX=2
55              ALF=ALFMUL*ALF
56              GO TO 15
57        C     MINIMUM HAS BEEN BOUNDED , MAKE N SEARCH ITERATIONS
58         30   TEMP=X2
59              X2=ALFSAV
60              ALFSAV=TEMP
61              TEMP=F2
62              F2=F
63              F=TEMP
64              IF(NPRINT)80,36,80
65        80    WRITE(6,250)
66         250  FORMAT(1HQ)
67         36   CALL QUAD(X1,X2,ALFSAV,ITER,KEY,F,F1,F2)
68              IF(KEY-4)27,37,99
69         37   IF(NPRINT)39,38,39
70        39    WRITE(6,40)
71         40   FORMAT(1HF)
72         38   CALL FIBMIN(X1,X2,ALFSAV,ITER,KEY,F,F1,F2)
73              IF(KEY-7)27,36,36
74         99   JUMP=1
75              GO TO 27
76        15    ALFSAV=ALFSAV+ALF
77        27    DO 21 J=1,N
78        21    X(J)=XSAVE(J)+ALFSAV*S(J)
79              IF (ALFSAV.LE..0000001) GO TO 25
80              IF(JUMP-1)26,25,26
81         25   IF(NPRINT)81,26,81
82        81    WRITE(6,24)
83         24   FORMAT(1HG)
84              KEY=7
85        26    RETURN
86        C     EXIT IF F HAS DECREASED INSIGNIFICANTLY
87         19   IF(ABS(F/FSAVE)-ERROR)11,10,10
```

```
     88      10     JUMP=0
     89             RETURN
     90      C      FORM H MATRIX VIA FLETCHER-POWELL
     91      11     DO 7 J=1,N
     92             SIG(J)=ALFSAV*S(J)
     93      7      DG(J)=G(J)-GSAVE(J)
     94             CALL MATMUL(SIG,1,N,DG,1,DEM,1.,1,1,1)
     95             CALL MATMUL(SIG,N,1,SIG,N,A,DEM,1,1,20)
     96             CALL MATMUL(DG,1,N,H,N,B,1.,1,20,20)
     97             CALL MATMUL(B,1,N,DG,1,DEM,1.,20,1,1)
     98             CALL MATMUL(DG,N,1,B,N,C,1.,1,20,20)
     99             CALL MATMUL(H,N,N,C,N,B,DEM,20,20,20)
    100             DO 8 J=1,N
    101             DO 8 K=1,N
    102      8      H(J,K)=H(J,K)+A(J,K)-B(J,K)
    103             JUMP=-1
    104             NGRAD=1
    105             GO TO 18
    106             END
END OF FILE


$COPY FROM *SOURCE* TO -QUAD
$LIST -QUAD
      1      C
      2             SUBROUTINE QUAD(XA,XC,XMIN,ITER,KEY1,F,FA,FC)
      3      C
      4             IF(F)21,21,30
      5       30    KEY=KEY1-1
      6             GO TO(100,300,100,100,100,100),KEY
      7       100   XAS=XA**2
      8             XCS=XC**2
      9             XB=XMIN
     10             XBS=XB**2
     11             FB=F
     12             J=0
```

```
      21    KEY1=KEY1+I
      2     IF(KEY1-4)4,23,23
      23    XMIN=XB
            ITER=ITER-J
            F=FB
            RETURN
      4     XD=.5*((XBS-XCS)*FA+(XCS-XAS)*FB+(XAS-XBS)*FC)
            XD=XD/((XB-XC)*FA+(XC-XA)*FB+(XA-XB)*FC)
            IF(XD-XC)90,90,21
      90    IF(XA-XD)91,91,21
      91    IF(ITER)89,21,89
      89    XDS=XD**2
            XMIN=XD
            RETURN
      300   FD=F
      22    IF(FD-FB)3,3,19
      19    IF(J)21,21,18
      18    ITER=0
            KEY1=KEY1+2
            GO TO 21
      3     IF(XD-XB)9,9,8
      8     FA=FB
            XA=XB
            XAS=XBS
            GO TO 10
      9     FC=FB
            XC=XB
            XCS=XBS
      10    FB=FD
            XB=XD
            XBS=XDS
            J=J+1
            IF(J-ITER)2,21,2
            END
END OF FILE
```

```
$COPY FROM *SOURCE* TO -MATMUL
$LIST -MATMUL
      1      C
      2            SUBROUTINE MATMUL(A,N,M,B,LL,C,DIV,NROW1,NROW2,NROW3)
      3      C
      4            DIMENSION A(1),B(1),C(1)
      5            DO 2 L=1,LL
      6            DO 2 J=1,N
      7            JJ=J+NROW3*(L-1)
      8            C(JJ)=0.
      9            DO 1 K=1,M
     10            JK=J+(K-1)*NROW1
     11            KL=K+(L-1)*NROW2
     12       1    C(JJ)=C(JJ)+A(JK)*B(KL)
     13       2    C(JJ)=C(JJ)/DIV
     14            RETURN
     15            END
END OF FILE


$COPY FROM *SOURCE* TO -FIBMIN
$LIST -FIBMIN
      1      C
      2            SUBROUTINE FIBMIN(X1,X2,XMIN,ITER,KEY1,F,F1,F2)
      3      C
      4      C*****THIS SUBROUTINE MINIMIZES A FUNCTION F BY A FIBONACCI SEARCH
      5      C     XMIN IS THE VALUE RETURNED AS A MIN, N IS THE NUMBER
      6      C     OF ITERATIONS MADE, ALF1 IS THE WIDTH OF THE ORIGINAL INTERVAL
      7      C     F IS THE VALUE OF FUNCTION AT XMIN
      8      C     XA AND XB ARE SEARCH POINTS AND FA AND FB ARE FUNCTION VALUES
      9      C     ORIGINALLY XMIN IS THE GREATER LIMIT OF THE BOUNDED INTERVAL
     10            KEYD=KEY1-3
     11            GO TO(100,200,300),KEYD
     12      100   IF(ITER)23,23,22
     13       23   KEY1=KEY1+3
```

```
14              RETURN
15        22    IY1=1
16              IY2=1
17              KEY1=KEY1+1
18           2  J=0
19        C     CALCULATE APPROPRIATE FIBONACCI NUMBERS
20        30    DO 3 I=1,ITER
21              ITEMP=IY2
22              IY2=IY2+IY1
23           3  IY1=ITEMP
24              Y1=IY1
25              Y2=IY2
26        C     DETERMINE FIRST SEARCH POINT
27           1  XA=X1+(X2-X1)*Y1/(Y1+Y2)
28              GO TO 400
29        C     DETERMINE NEXT SEARCH POINT AND VALUE OF FUNCTION
30        300   IF(KEY)14,14,13
31        13    FA=F
32              GO TO 6
33        14    FB=F
34           6  J=J+1
35        C     DETERMINE MINIMAL SEARCH POINT
36           8  IF(FA-FB)4,4,5
37           4  X2=XB
38              F2=FB
39              KEY = 1
40              XB=XA
41              FB=FA
42        C     DETERMINE NEXT SEARCH POINT AND VALUE OF FUNCTION
43              XA=X1+X2-XB
44        400   XMIN=XA
45        21    IF(J-ITER)20,9,9
46        20    RETURN
47         200  FA=F
48        12    KEY1=KEY1+1
49              GO TO 500
```

```
    50           5 X1=XA
    51             F1=FA
    52             XA=XB
    53             FA=FB
    54         500 KEY=-1
    55             XB=X2-XA+X1
    56             XMIN=XB
    57             GO TO 21
    58         9   KEY1=KEY1+1
    59       C     RETURN APPROPRIATE VALUE FOR XMIN
    60             ITER=0
    61             IF(KEY)10,10,11
    62          10 XMIN=XA
    63             F=FA
    64             RETURN
    65          11 XMIN=XB
    66             F=FB
    67             RETURN
    68             END
END OF FILE
```

DISTRIBUTION LIST

	No. of Copies
National Security Agency Ft. George G. Meade, Maryland 20755	20
Technical Library Dir. of Defense Research & Engineering Rm. 3E-1039, The Pentagon Washington, D. C. 20301	1
Defense Intelligence Agency Attn: DIARD Washington, D. C. 20301	1
Director National Security Agency Attn: C31 Fort George G. Meade, Maryland 20755	2
Naval Ships Systems Command Attn: Code 20526 (Technical Library) Main Navy Building, Rm. 1528 Washington, D. C. 20325	1
Naval Ships Systems Command Attn: Code 6179B Department of the Navy Washington, D. C. 20360	1
Director U. S. Naval Research Laboratory Attn: Code 2027 Washington, D. C. 20390	2
Commanding Officer and Director U. S. Navy Electronics Laboratory Attn: Library San Diego, California 92152	1

DISTRIBUTION LIST (Cont.)

	No. of Copies
Commander U. S. Naval Ordnance Laboratory Attn: Technical Library White Oak, Silver Spring, Maryland 20910	1
Dir. Marine Corps Landing Force Dev Ctr Attn: C-E Division Marine Corps Schools Quantico, Virginia 22134	1
Commandant of the Marine Corps (Code AO2F) Headquarters, U. S. Marine Corps Washington, D. C. 20380	1
Rome Air Development Center (EMTLD) Attn: Documents Library Griffiss Air Force Base, New York 13440	1
U. S. Army Security Agency Test & Evaluation Center Fort Huachuca, Arizona 85613 Code IAOVT	1
Electronic Systems Division (TRI) L. G. Hanscom Field Bedford, Massachusetts 01730	2
U. S. Air Force Security Service Attn: TSG, VICE Attn: ESD San Antonio, Texas 78241	1
ADTC (ADBRL-2) Eglin Air Force Base, Florida 32542	1
Headquarters, AFSC Attn: SCTSE Bolling AFB, D. C. 20332	1
Air University Library (3T) Maxwell Air Force Base, Alabama 36112	1
HQ, USAF Tactical Air Recon Ctr (TAC) Department of the Air Force Shaw Air Force Base, South Carolina 29152	1

DISTRIBUTION LIST (Cont.)

	No. of Copies
Chief of Research and Development Department of the Army Washington, D. C. 20315	2
Commanding General U. S. Army Materiel Command Attn: R&D Directorate Washington, D. C. 20315	2
Redstone Scientific Information Center Attn: Chief, Document Section U. S. Army Missile Command Redstone Arsenal, Alabama 35809	3
Headquarters U. S. Army Weapons Command Attn: AMSWE-RER Rock Island, Illinois 61201	1
Commanding Officer U. S. Foreign Science & Tech Ctr Attn: AMXST-RD-R, Munitions Bldg Washington, D. C. 20315	1
Director, National Security Agency Attn: N-2, Mr. Sherwood Fort George G. Meade, Maryland 20755	1
Commanding Officer Aberdeen Proving Ground Attn: Technical Library, Bldg. 313 Aberdeen Proving Ground, Maryland 21005	2
Headquarters U. S. Army Materiel Command Attn: AMCMA-RM/3 Washington, D. C. 20315	2
Commanding General U. S. Army Combat Developments Command Attn: CDCMR-E Fort Belvoir, Virginia 22060	1

DISTRIBUTION LIST (Cont.)

	No. of Copies
Commanding Officer U. S. Army Combat Developments Command Communications-Electronics Agency Fort Monmouth, New Jersey 07703	3
Commander U. S. Army Research Office (DURHAM) Box CM-DUKE Station Durham, North Carolina 27706	1
Commanding Officer U. S. Army Sec Agcy Combat Dev ACTV Arlington Hall Station Arlington, Virginia 22212	1
U. S. Army Security Agency Attn: DCSR&R Arlington Hall Station Arlington, Virginia 22212	1
U. S. Army Security Agcy Processing Ctr Attn: IAVAPC-R&D Vint Hill Farms Station Warrenton, Virginia 22186	1
Technical Support Directorate Attn: Technical Library Bldg 3330, Edgewood Arsenal Maryland 21010	1
U. S. Army Research & Dev Command Branch Library, Bldg 5695 Nuclear Effects Laboratory Edgewood Arsenal, Maryland 21010	2
Harry Diamond Laboratories Attn: Library Connecticut Avenue and Van Ness Street Washington, D. C. 20438	1
Commandant U. S. Army Air Defense School Attn: C&S Dept. MSL SCI DIV Fort Bliss, Texas 79916	1

DISTRIBUTION LIST (Cont.)

	No. of Copies
Commanding General U. S. Army Electronic Proving Ground Attn: Technical Information Center Fort Huachuca, Arizona 85613	1
Asst. Secretary of the Army (R&D) Department of the Army Attn: Deputy Asst. for Army (R&D) Washington, D. C. 20315	1
Commanding Officer U. S. Army Limited War Laboratory Aberdeen Proving Ground, Md. 21005	1
CH, Special Techniques Division Unconventional Warfare Department U. S. Army Special Warfare School Fort Bragg, North Carolina 28307	1
USAECOM Liaison Office U. S. Army Electronic Proving Ground Fort Huachuca, Arizona 85613	1
Office, AC of S for Intelligence Department of the Army Attn: ACSI-DSRS Washington, D. C. 20310	1
Chief, Mountain View Office EW Lab USAECOM Attn: AMSEL-WL-RU P. O. Box 205 Mountain View, California 94042	1
Chief, Intelligence Materiel Dev Office Electronic Warfare Lab, USAECOM Fort Holabird, Maryland 21219	1
Chief Missile Electronic Warfare Tech Area EW Lab, USA Electronics Command White Sands Missile Range, N. M. 88002	1

DISTRIBUTION LIST (Cont.)

	No. of Copies
Headquarters U. S. Army Combat Developments Command Attn: CDCLN-EL Fort Belvoir, Virginia 22060	1
USAECOM Liaison Officer MIT, Bldg. 26, Rm. 131 77 Massachusetts Avenue Cambridge, Mass. 02139	1
Commanding General U. S. Army Electronics Command Fort Monmouth, New Jersey 07703 Attn:	
AMSEL-EW	1
AMSEL-PP	1
AMSEL-IO-T	1
AMSEL-GG-DD	1
AMSEL-RD-LNJ	1
AMSEL-XL-D	1
AMSEL-NL-D	1
AMSEL-VL-D	1
AMSEL-KL-D	1
AMSEL-HL-CT-D	3
AMSEL-BL-D	1
AMSEL-WL-S	3
AMSEL-WL-S (office of record)	1
AMSEL-SC	1
Dr. T. W. Butler, Jr., Director Cooley Electronics Laboratory The University of Michigan Ann Arbor, Michigan 48105	1
Cooley Electronics Laboratory The University of Michigan Ann Arbor, Michigan 48105	16

Security Classification

DOCUMENT CONTROL DATA - R & D

(Security classification of title, body of abstract and indexing annotation must be entered when the overall report is classified)

1. ORIGINATING ACTIVITY *(Corporate author)*

Cooley Electronics Laboratory
University of Michigan
Ann Arbor, Michigan 48105

2a. REPORT SECURITY CLASSIFICATION

Unclassified

2b. GROUP

3. REPORT TITLE

High-Frequency Transistor Modeling for Circuit Design

4. DESCRIPTIVE NOTES *(Type of report and inclusive dates)*

Technical Report No. 205, May 1971

5. AUTHOR(S) *(First name, middle initial, last name)*

A. B. Macnee and R. J. Talsky

6. REPORT DATE	7a. TOTAL NO. OF PAGES	7b. NO. OF REFS
May 1971	72	8

8a. CONTRACT OR GRANT NO.	9a. ORIGINATOR'S REPORT NUMBER(S)
DAAB07-68-C-0138	TR205
b. PROJECT NO. 1 H0 21101 A04 01 02	
c.	9b. OTHER REPORT NO(S) *(Any other numbers that may be assigned this report)*
d.	ECOM-0138-19-T 014820-19-T

10. DISTRIBUTION STATEMENT

11. SUPPLEMENTARY NOTES

12. SPONSORING MILITARY ACTIVITY

U. S. Army Electronics Command
Fort Monmouth, New Jersey 07703
Attn: AMSEL-WL-S

13. ABSTRACT

It has been found that hybrid-pi or high-frequency T are inadequate high-frequency models for certain transistor types even though the models are supplemented by reasonable extrinsic elements. The hybrid-pi can be modified to model these transistors by replacing the $r_\pi C_\pi$ circuit by an RC ladder. Using a computer optimization program an optimal, N-lump model is generated. For the 2N918 transistor a two-lump model extends the frequency range of the hybrid-pi model to $f_T/2$. Typical circuit examples show most of the improvement in model performance can be obtained with a two-lump model.

14. KEY WORDS	LINK A		LINK B		LINK C	
	ROLE	WT	ROLE	WT	ROLE	WT
High-frequency transistor modeling Hybrid-pi models High-frequency T Computer optimization program						